Quarterly Journal of the Royal Meteorological Society
A journal of the atmospheric sciences and physical oceanography

The performance of the CoMorph-A convection package in global simulations with the Met Office Unified Model

Journal:	*QJRMS*
Manuscript ID	QJ-23-0172.R2
Wiley - Manuscript type:	Research Article
Date Submitted by the Author:	08-May-2024
Complete List of Authors:	Lock, Adrian; Met Office Whitall, Michael; Met Office, Atmospheric Parameterisations and Processes Stirling, Alison; Met Office Williams, Keith; Met Office Lavender, Sally; University of Southern Queensland, Centre for Applied Climate Sciences; Met Office, Morcrette, Cyril; Met Office Field, Paul; Met Office Martin, Gill; Met Office, Cliamte Research Willett, Martin; Met Office, Met R & D Heming, Julian; Met Office, Foundation Science Matsubayashi, Kengo; JMA
Keywords:	Convection < 3. Physical phenomenon, parametrization, Global < 2. Scale, evaluation, Unified Model, General circulation model experiments < 1. Tools and methods, Numerical methods and NWP < 1. Tools and methods, Atmosphere < 4. Geophysical sphere
Country Keywords:	United Kingdom Of Great Britain And Northern Ireland, Japan, Australia

ORIGINAL ARTICLE

Journal Section

The performance of the CoMorph-A convection package in global simulations with the Met Office Unified Model

A. P. Lock[1] | M. Whitall[1] | A. J. Stirling[1] | K. D. Williams[1] | S. L. Lavender[2,1] | C. Morcrette[1] | K. Matsubayashi[3] | P. R. Field[1] | G. Martin[1] | M. Willett[1] | J. Heming[1]

[1]Met Office, FitzRoy Way, Exeter, EX1 3PB.

[2]Centre for Applied Climate Sciences, University of Southern Queensland, Toowoomba, Australia.

[3]Japan Meteorological Agency, Minato City, Tokyo, Japan

Correspondence
Met Office, FitzRoy Way, Exeter, EX1 3PB.
Email: adrian.lock@metoffice.gov.uk

Funding information

The impact on global simulations of a new package of physical parametrizations in the Met Office Unified Model is documented. The main component of the package is an entirely new convection scheme, CoMorph. This has a mass-flux structure that allows initiation of buoyant ascent from any level and the ability for plumes of differing originating levels to coexist in a grid box. it has a different form of closure, where the mass-flux of initiation is dependent on local instability, and an implicit numerical solution for detrainment that yields smooth timestep behaviour. The scheme is more consistently coupled to the cloud, microphysics and boundary layer parametrizations and, as a result, significant changes to these have also been made. The package, called CoMorph-A, has been tested in a variety of single-column and idealised regimes. Here we test it in global configurations and evaluate it against observations using a range of standard metrics. Overall it is found to perform well against the control. Biases in the climatologies of the radiative fluxes are significantly reduced across the tropics and sub-tropics, tropical and extratropical cyclone statistics are improved and the MJO and other propagating tropical waves are strengthened. It also improves overall scores in NWP trials, without revisions to the data assimilation. There is still work to do to improve the diurnal cycle of precipitation over land, where the peak remains too close to the middle of the day.

KEYWORDS
Convection, parametrization, global, evaluation, Unified Model

1 | INTRODUCTION

The representation of convection in general circulation models (GCMs) has long been recognised as having a central control on model performance, not only influencing the distribution of precipitation, but also global circulation patterns, and the resulting cloud and radiative fluxes that respond to them (e.g. Xie et al. (2012), Holloway et al. (2014) and Sherwood et al. (2014)). Common to many GCMs, the Unified Model has previously used a mass-flux scheme based on simplified Arakawa-Schubert principles (Arakawa and Schubert (1974)), which was devised by Gregory and Rowntree (1990), and used largely predefined profiles for entrainment, a simple link to detrainment, along with a CAPE-based closure. While this scheme and its subsequent variants (e.g. Derbyshire et al. (2011), Walters et al. (2019), Willett and Whitall (2017)) has been able to produce good mean atmospheric states (e.g. Walters et al. (2019)), it has had difficulty generating appropriate coupling between convection and the model dynamics. This is seen in a range of emergent atmospheric phenomena that rely on the close feedbacks between convection and the larger-scale dynamics. Examples, in the UM and many other GCMs, include the insufficient strength and progression of the MJO, (e.g. Klingaman and Woolhough (2013) and Ahn et al. (2020)); the low amplitude of convectively-coupled Kelvin and other equatorial waves (Vitart et al. (2007), Janiga et al. (2018) and Dias et al. (2023)); the limited strength and frequency of African Easterly waves (Bain et al. (2014)), and their link to mesoscale convective systems (Tomassini (2018)). At the heart of the difficulty in representing these phenomena (in the current and earlier generations of GCM resolutions), lies the need to enable appropriate positive feedbacks to develop between convection and its parent dynamics, while keeping the model stable by preventing the emergence of convective instability onto the resolved grid.

The need for model stability has similarly made an apparently straightforward problem of capturing the correct timing (and amplitude) of the diurnal cycle of convection over land (Yang and Slingo (2001), Christopoulos and Schneider (2021), and Tao and et al (2024)) a challenge to rectify, as delaying convective activity for too long in the presence of a convectively-unstable atmosphere risks instability reaching the scale of the model grid, and the resolved dynamics responding accordingly.

Mass-flux schemes that use a closure based on convective available potential energy (CAPE) have success in keeping the resolved model stable (e.g. Walters et al. (2019)), but the use of such a vertical integral of convective instability in the troposphere to determine the mass flux at cloud base produces a disconnection between the conditions required in the boundary layer to trigger convection (for example, enough kinetic energy to overcome layers of convective inhibition), and those linked to its response (e.g.Mapes (2000) and Fletcher and Bretherton (2010). This can lead to numerical intermittency of CAPE-closed schemes across the timestep, as the CAPE-closure can create enough convective inhibition to prevent triggering on the next timestep (e.g. Klingaman et al. (2017)). Furthermore closures based on CAPE desensitise convective activity to local variations in the vertical thermodynamic profile, making it harder for the convection scheme to respond in tandem with the resolved dynamics (Whitall et al. (2022)). In addition, the use of predefined profiles for entrainment leads to somewhat inflexible representations of the mass-flux shape, making smooth transitions between different convective states hard to achieve.

These limitations, along with embedded decisions in the convection-scheme code about the levels of convective initiation, and the number of updraughts allowed at any one level, have motivated the development of an entirely new convection scheme called CoMorph, Whitall et al. (2022). This scheme provides a much more flexible architecture that enables complexity to be built in as required, and with the aim of creating a scheme that is better connected to the underpinning physical processes that drive convective activity.

CoMorph-A represents a first implementation of this scheme, designed for a global package, with the priorities of this version being to improve the coupling between convection and the resolved dynamics, as well as the consistency of interaction with other physics parametrisations. Numerous tests of the scheme under controlled forcing conditions have been conducted, for example in a Single Column Model (Whitall et al. (2022)), and for a range of case studies in the Idealised MetUM (a 3D, Cartesian, bi-periodic version of the Met Office Unified Model, Lavender et al. (2024)), with promising behaviour across a range of regimes. The coupling of the scheme to the dynamics has also been investigated (Daleu et al. (2023)), again highlighting the significant advances and potential of the new scheme. Zhu et al. (2023b) have also investigated the impacts of CoMorph-A in global simulations, focusing on the Indo-Pacific and Australian regions, finding significant benefits.

This paper introduces the CoMorph-A and accompanying control package configurations of the Met Office Unified Model (UM) in sections 2 and 3. To evaluate the impacts and performance of the new package, we follow the standard testing procedure as laid out in Walters et al. (2019), and evaluate the performance of the same configuration in both climate and numerical weather prediction (NWP). The climate evaluation in section 4 uses 20 years of simulation using AMIP specified sea-surface temperatures and sea ice. For NWP, while we have also run forecast only simulations, as in Walters et al. (2019), in section 5 we present verification from two 3-month long cycling forecast and analysis trials of the CoMorph-A package, so including 4DVar data assimilation (albeit without updating the error covariance and other assimilation statistics).

2 | CONTROL MODEL

The control configuration of the Met Office Unified Model (MetUM) used in this study is GA8GL9, which is based on GA7GL7 (Walters et al. (2019)) but incorporates new developments intended for the next release that will be documented in detail elsewhere. GA8GL9 is the basis for the current operational NWP at the Met Office at the time of writing. The main changes since GA7GL7 are:

- a package of changes related to model drag, described in Williams et al. (2020)
- revised parametrizations in the grid-scale microphysics for riming and the depositional growth of ice (Furtado and Field (2017))
- a new "multigrid" dynamical solver
- reduced drag at high wind speeds over the sea which improves forecasts of tropical cyclones at higher model resolutions than discussed here
- significant modifications to the existing massflux convection scheme

To give a brief description of GA7GL7, the ENDGame dynamical core uses a semi-implicit semi-Lagrangian formulation to solve the non-hydrostatic, fully compressible deep-atmosphere equations of motion (Wood et al. (1999)). The grid-scale microphysics scheme (i.e., that which operates on the gridded prognostic variables) is single-moment with prognostic rain and ice, based on Wilson and Ballard (1999). The parametrisation of the fraction of the grid box which is covered by cloud, and the amount and phase of condensed cloud water it contains, is the prognostic cloud fraction and prognostic condensate (PC2) scheme (Wilson et al. (2008a), Wilson et al. (2008b)). The parametrization of radiative transfer (solar, shortwave (SW), and thermal, longwave (LW)) uses the SOCRATES scheme (Edwards and Slingo (1996); Manners et al. (2015) The turbulence scheme uses a first-order closure from Lock et al. (2000), mixing adiabatically conserved heat and moisture variables, momentum and tracers, using non-local profiles of diffusion coefficients within convective boundary layers and an explicit parametrization of entrainment across their top. In the control simulations the parametrization of sub-grid-scale transport of heat, moisture and momentum associated with cumulus clouds is a mass-flux convection scheme based on Gregory and Rowntree (1990). Three separate classes of convection are represented. First a diagnosis is made to determine whether convection is possible from the boundary layer, and its potential depth, using an adiabatic undilute parcel ascent, which then triggers either a shallow or deep convection scheme. Any remaining instability to moist ascent identified above the boundary layer and the top of any shallow or deep convection is handled by a mid-level scheme. Each component involves different parametrization of processes such as entrainment and detrainment from the plume, together with separate closures (based on the surface buoyancy flux for shallow convection and CAPE for mid-level and deep).

Of the modifications to the GA7GL7 convection scheme used in our control, two are of most relevance here. The first, described in Willett and Whitall (2017), is to relate the entrainment rate in the deep component of the scheme to the amount of recent convective activity, as measured by an advected prognostic, similar to Mapes and Neale (2011). The source term for this is scaled on the surface convective precipitation rate, expanded to three dimensions using the current convective temperature increment profile, and decays with a 3 hour timescale. In this way the scheme is given a short term memory of previous convective activity, thereby allowing evolution of convective clouds over finite time scales. The second significant change from GA7GL7 is to time-smooth the heat and moisture increments from the convection scheme over a timescale of 45 minutes. This is to reduce the impact of strong time-step-level intermittency in the scheme (see section 4) on the resolved scale dynamics. Note that this increment smoothing is *not* used with the CoMorph-A package.

Finally, note that most of these parametrizations have undergone significant modification between their original references, as above, and GA7GL7 and the reader is referred to Walters et al. (2019) for more detail.

3 | COMORPH-A PACKAGE

An important aspect of the new convection parametrization, CoMorph, is that it is directly coupled to, and hence strongly dependent on, other aspects of the model physics. In particular, the presence or otherwise of cloud strongly affects the initial sources of mass, and the turbulence statistics from the boundary layer scheme determine the initial characteristics of the plume. Initial development in a single-column version of the MetUM highlighted unwanted sources of intermittency and sporadic unrealistic behaviour at the time step and grid level. For the proper functioning of the CoMorph convection scheme, as well as for the overall performance, it was therefore necessary to make significant changes to several other aspects of the physical parametrizations that will be described in this section. Together these then form the CoMorph-A package.

3.1 | CoMorph convection scheme

The control convection scheme is replaced by the entirely new scheme, CoMorph. Details are given in Whitall et al. (2022) but we give a summary here.

As in the control, the CoMorph scheme uses the massflux approach to parametrize the effects of subgrid cumulus convection but CoMorph has an entirely new code structure, to allow greater flexibility, and many differences in approach with additional physical processes included. There is no external closure in CoMorph. Instead, the massflux initiated from any locally unstable model grid-level is proportional to the relative size of the local environment lapse rate to that of a test parcel. Where the prognostic cloud fraction parametrization identifies a grid box as having partial cloud cover, separate initiation calculations are made in the saturated and unsaturated air and these are combined using area weighting by the cloud fraction.

The rate of entrainment scales with an inverse parcel radius, i.e.,

$$\epsilon = \frac{\alpha_{ent}}{R} \tag{1}$$

where α_{ent} is a dimensionless parameter currently set to 0.2. The parcel radius, R, is based on a turbulence length-scale in the parcel's source-layer given by $R = a_L K_M / \sigma_w$, where K_M is the momentum diffusivity in the boundary layer scheme and a_L a constant taken to be 0.45; $\sigma_w = (K_M/\tau)^{0.5}$ is a turbulent velocity scale where τ is a turbulent timescale, see Van Weverberg et al. (2016). Initial testing in the global model, however, found this simple formulation was insufficient to remove instability fast enough under all circumstances and so an additional scaling was introduced, increasing a_L based on an ad-hoc linear function of the previous time step's precipitation rate (up to a factor of 2 for a precipitation rate above approximately 35 mm per day). Qualitatively this can be viewed as allowing the updraft size to respond to the organisation of convection via precipitation leading to the formation of cold pools and subsequent initiation of larger-scale updraughts (Mapes and Neale (2011)). The parcel radius increases with height through entrainment by assuming the mass-flux is carried by a fixed number-flux of spherical thermals whose radii increase consistent with the increase in volume of each thermal.

The detrainment rate is modelled as removing the non-buoyant part of an assumed distribution of buoyancy within the bulk plume, informed by separate parcel ascent calculations for parcel mean and less dilute core properties. Importantly, this detrainment calculation is solved implicitly, in which the convective heating of the environment (as well as the other model increments through the timestep) is accounted for in the calculation of the parcels' buoyancy and therefore the proportion of the buoyancy distribution that is detrained.

The initiating parcel mean properties are calculated separately within each clear or cloudy sub-grid region, as with massflux initiation, and then averaged together weighted by their respective initiating massfluxes. The in-region properties are taken as just saturated and neutrally buoyant and then given a perturbation, ϕ', linked to the parametrized turbulent flux ($\phi' = \alpha_t \overline{w'\phi'}/\sigma_w$ with $\alpha_t = 1/3$ and ϕ being temperature, water vapour mixing ratio and the horizontal wind components). Because the parcel core is representing the most extreme tail of the distribution of sub-grid fluctuations, the core property perturbations are scaled up by a factor of 3.

As with the control, CoMorph uses a massflux representation of momentum transport by convection that also includes the effects of cloud pressure-gradients on the flow within the cloud (e.g., Kershaw and Gregory (1997)).

Importantly, CoMorph also includes a novel in-parcel bulk microphysics scheme for the generation of hydrometeors. These hydrometeors are then passed on the model-level where they leave the parcel (through detrainment and a fall-out flux) to the grid-scale microphysical variables. This can be achieved because, as in the control, the model's grid-scale (Wilson-Ballard) microphysics scheme prognoses the mass concentration of each hydrometeor species so convection can now provide an additional source term for these prognostics. Their fall to the surface, and any interactions on the way down, is modelled by the Wilson-Ballard scheme which therefore improves the consistency of treatment of precipitation between that generated through convective processes and that through larger, resolved scale ones. Note that diagnostically this means there is no longer any separation into convective or large-scale precipitation, just precipitation. In order for convection to modify rain mass and area fraction consistently a prognostic precipitation area fraction is introduced and passed to the large-scale microphysics. In addition to cloud liquid water, ice and rain, CoMorph itself includes graupel, which is not represented explicitly in the control model, being largely a feature of deep convection which is entirely parametrized there, but passing CoMorph's graupel to the large-scale's single ice variable led to far too excessive build-up of cloud ice in the tropics and so the large-scale microphysics' prognostic graupel was also included in the CoMorph-A package (following the configuration already used in the regional configurations of the UM, see Bush et al. (2020)). This initial implementation of a microphysics scheme in CoMorph is relatively simple, prescribing a representative number concentration for each hydrometeor species in order to calculate an effective particle size and thence fall speeds, accretion rates and other exchanges between hydrometeor classes. Crucially this allows the parcel (and detrained air) to become supersaturated with respect to ice, whereas the convection scheme in the control adjusts the parcel fully to ice-saturation when below the melting point temperature.

CoMorph is also written in terms of mixing ratios of water vapour and condensate (while the control convection scheme uses specific quantities). This has then allowed all the model's physics schemes to move across to using mixing ratios, consistent with the dynamical core, and so avoid conversions in moving between different parts of the model which allows global water conservation errors to be reduced to negligible levels.

In summary, the key aspects of the CoMorph convection scheme are:

- it is a single unified scheme for all convective regimes
- it is closely integrated with the rest of the model physics, giving greater physical consistency
- massflux is initiated through local moist instability leading to a much tighter coupling with the resolved dynamics of the model
- close attention has been paid to the numerical methods used, with substantial aspects solved implicitly, and this leads to a smooth temporal behaviour

- it includes a microphysical representation of cloud process in its updraughts and precipitation is passed directly to the prognostic grid-scale microphysical variables instead of being rained out diagnostically, thereby improving consistency of treatment of microphysical processes in the model

3.2 | Other model changes

3.2.1 | Cloud scheme

The impact of triggering CoMorph from either saturated or unsaturated air makes it sensitive to the diagnosis of the fraction of the grid box that is cloudy. In the process of developing CoMorph, several aspects of the PC2 cloud scheme were discovered to be excessively sensitive to small perturbations. Largely motivated, then, by a desire to reduce the timestep level variability of convection, the following changes were made to the PC2 cloud scheme:

- to ensure the cloud is consistent with the thermodynamic profiles at the point in the timestep where these are passed to CoMorph, the PC2 homogeneous forcing calculation from advection is moved from the end of the timestep to just after the advection calculation (which is called before convection) and new calls to the PC2 initiation and checking algorithms are added before the call to CoMorph
- the “BiModal” scheme of Weverberg et al. (2021) is used for initiation of cloud within PC2 (because of its more realistic treatment of subgrid variability), together with using that initiated cloud as a minimum cloudiness (cloud fraction and liquid water content) at every grid-point on every timestep (in the control the cloud has to dissipate completely before initiation is triggered which can lead to sudden large changes in cloud fraction)
- for consistency, the pressure change experienced by the environment as it undergoes convectively forced subsidence is used to drive the homogeneous forcing of cloud, following the same method as for resolved advection (Wilson et al. (2008a)), a process not treated explicitly in the control
- an implicit numerical method is introduced to calculate the PC2 term for the erosion of cloud, which depends on the cloud fraction (see Morcrette (2012)), such that the erosion rate applied is consistent with the cloud-fraction that will occur after the erosion increment has been added on
- the method of Morcrette (2020) is used to ensure that the PC2 cloud scheme produces reasonable magnitude cloud fraction increments in the limit of small condensate amounts

3.2.2 | Cloud microphysics

As discussed in section 3.1, the main changes to microphysics are to include graupel as a prognostic variable, which allows for the explicit representation of a second, more dense ice category, and to include a fractional area of precipitation so as to discriminate convectively generated rain that occupies a small fraction of the grid box from that generated by large-scale processes. Another, more minor, improvement is to relax the shallow atmosphere assumption in the calculation of flux divergences, and so be consistent with the rest of the model, which improves local conservation of water.

3.2.3 | Fountain Buster

In the absence of sufficient lateral subgrid mixing, the MetUM has been found susceptible to the formation of near-grid-scale flow structures that, combined with the lack of inherent conservation with semi-implicit semi-Lagrangian advection, leads to significant conservation errors. This problem can be illustrated by considering an idealised up-draught in a single grid-column with continuity requiring a convergent in-flow in lower levels. The interpolation of the Arakawa C staggered horizontal wind fields onto scalar points, however, strongly reduces resolved lateral convergence from surrounding points into grid-scale vertically ascending plumes. As a result, the vertical transport of, for example, water vapour away from the near surface is not compensated for by horizontal convergence of drier air into the plume from the sides, with the result that moisture can be transported vertically ad infinitum. Typically this is then manifested as extreme local precipitation accumulations. The use of a posteriori global conservation correction has been found to reduce these errors significantly (Bush et al. (2020)), but substantial local errors have been found to remain.

Here a post-hoc local correction is applied after the semi-Lagrangian scheme's interpolation to the departure point, in the form of the linear up-wind advection increments that arise from the convergent part of the flow that is removed when the horizontal wind components are interpolated to the scalar grid points for the departure point calculation. In more detail, first, at each lateral cell face a measure of the (assumed missing) convergent stagnation in-flow, S, is calculated. For example, for the west cell face of scalar point (i, j, k):

$$S_{\text{west}} = \frac{u_{i-1,j,k} - s_d u^{\theta}}{u_{i-1,j,k}} \tag{2}$$

where u^{θ} is a linear estimate of u at the scalar point. To ensure only the convergent part of the flow is accounted for, we ensure $0 < S_{\text{west}} < 1$, and to avoid making increments in reasonably well-resolved flows the tuning factor, s_d, is set to 2.

The fountain buster tendency for a scalar variable χ is then given by first-order upwind advection scaled by S, i.e.:

$$\begin{aligned} \frac{\Delta \chi_{i,j,k}}{\Delta t} &= S_{\text{east}} u^f_{i,j,k} \frac{\chi_{i+1,j,k} - \chi_{i,j,k}}{\Delta x} - S_{\text{west}} u^f_{i-1,j,k} \frac{\chi_{i,j,k} - \chi_{i-1,j,k}}{\Delta x} \\ &+ S_{\text{south}} v^f_{i,j-1,k} \frac{\chi_{i,j,k} - \chi_{i,j-1,k}}{\Delta y} - S_{\text{north}} v^f_{i,j,k} \frac{\chi_{i,j+1,k} - \chi_{i,j,k}}{\Delta y} \end{aligned} \tag{3}$$

where the superscript ^{f} denotes the wind interpolated (vertically) to the face centre of the scalar point. In (3) a regular cartesian grid has been used for simplicity but in the MetUM the appropriate metric variables are used. The fountain buster is applied to all advected scalar variables, so all moisture variables, tracers and the thermodynamic variable (dry virtual potential temperature).

3.2.4 | Turbulent mixing

A deliberate choice in the Lock et al. (2000) boundary layer scheme was to interface with the convection scheme at the lifting condensation level (LCL, diagnosed from the top of the surface layer), meaning that the boundary layer scheme would be entirely responsible for surface-driven mixing at least up to the LCL, from where the convection scheme would then be initiated and take over the transport into the free troposphere. With CoMorph, initiation can now occur at any level and so we take the opportunity to relax the requirement that the boundary layer scheme mix up to this definition of the LCL. We still use the Lock et al. (2000) undilute moist adiabatic parcel ascent method to diagnose the potential for cumulus convection but, in those regimes, now diagnose the top of the surface-driven turbulence diffusion profile as the point where the integral of diagnosed negative buoyancy flux is a fraction (0.05, see Walters et al. (2019)) of the vertical integral of the positive flux. Because we assume any transport within clouds will be carried by CoMorph, we use the unsaturated buoyancy flux in this calculation.

A second alteration to the boundary layer scheme is in the calculation of the buoyancy gradient used in the Richardson number (Ri). This is revised to reduce the mixing from the Ri-dependent part of the scheme across statically stable inversions, in particular where these cap a cloudy boundary layer. With the UM's Charney-Philips vertical grid staggering, Ri is required on the same grid-level as scalars (referred to as θ-levels), where the vertical gradient of horizontal momentum naturally falls. In the control, the gradients of liquid-ice static energy temperature and total water content are interpolated to θ-levels and that θ-level's cloud fraction used to obtain the buoyancy gradient. It is found that at cloudy θ-levels below a strong inversion this interpolation of the gradients, combined with a saturated buoyancy calculation, can lead to apparent instability. In the CoMorph-A package we calculate the buoyancy gradient locally (on ρ-levels) and interpolate that to the θ-levels. To calculate the saturated contribution to the buoyancy gradient on ρ-levels, an estimate of the vertical fraction of the grid containing saturated air is made from interpolating the supersaturation in the adjacent θ-levels. In this way the contribution from the ρ-level with strong gradients is typically largely unsaturated, leading to strong stability, which then remains stable when averaged with the saturated ρ-level with weak gradients below.

As with the Fountain Buster, the more active dynamics in the tropics arising from more organised convection with CoMorph also motivates enabling the Leonard terms (Hanley et al. (2019)), which include extra subgrid vertical fluxes that account for the tilting of horizontal flux into the vertical by horizontal gradients in vertical velocity. Including these terms helps to weaken a few occurrences of excessively strong resolved updraughts and precipitation in organised convective structures.

3.3 | Tuning of the top-of-atmosphere radiation

As with any major model developments, the initial simulations showed significantly worse biases than the control, both locally and globally in the top-of-atmosphere radiation. To reduce excessively weak outgoing longwave radiation (OLR) in the tropics, we increased the fall speeds for cloud ice by 20% (which increases the global mean OLR by around 1.5 Wm^{-1} and reduces the spatial root-mean-square error (rmse) against satellite climatology (see section 4) by 0.3 Wm^{-1}) and also removed a parametrization in PC2 that increased the ice cloud fraction through vertical wind shear that was not especially well justified physically (which increased the global mean OLR, by 0.5 Wm^{-1}, and reduced the rmse by 0.3 Wm^{-1}). In the shortwave (SW), the cloud forcing was initially too strong across most of the tropics. Several options are available that can reduce the reflectivity of clouds and we have made two revisions. The first was to the parameters in the Liu et al. (2008) spectral dispersion of the cloud droplet size distribution. As described in Mulcahy et al. (2018), the cloud droplet spectral dispersion as implemented in the control is given by

$$\beta = a\left(\frac{L}{N_d}\right)^b \tag{4}$$

where L is the cloud liquid water content and N_d the cloud droplet number concentration. In the control $a = 0.07$ and $b = -0.14$ while in the CoMorph-A package we use $a = 0.093$ and $b = -0.13$. These changes, that are small compared to the spread in the Liu et al. (2008) data, resulted in a reduction in global mean reflected SW of around 1.5 Wm^{-1}, whilst having almost no impact on OLR. Regionally the SW impact was strongest broadly across the marine sub-tropics and gave a reduction in spatial rmse of around 1 Wm^{-1}. Our second tuning, to further reduce the reflectivity of clouds, was to increase a parameter in the fractional standard deviation of liquid clouds (equal to the standard deviation of cloud water content in a grid box divided by its mean value, see Hill et al. (2015)) from 1.6 to 1.65, which reduced the global mean reflected SW by around 0.7 Wm^{-1} and the spatial rmse by 0.25 Wm^{-1}. Note, though, that the impacts of these last two changes would certainly be different if implemented in the reverse order.

It is important to remember that this tuning is a critical step in any new physics package and was, of course, also done for the control configuration. Hence the impacts discussed in section 4 should be viewed as resulting from the CoMorph-A package as a whole.

3.4 | Cost

There is a marginal increase in the CPU time with CoMorph-A of roughly 5% over the control of which a substantial part will be the new prognostic graupel - tests with just the convection scheme reverted to that in the control show a similar increase indicating the CoMorph convection scheme itself is cost neutral.

4 | RESULTS IN AMIP

We evaluate the climatology of the CoMorph-A package using AMIP simulations at N96 resolution (around 135 km grid spacing in mid-latitudes). Given the main change is to the convection parametrization, we start by looking in Fig. 1 at the impact on the annual mean precipitation. The most systematic change is to have increased rain over tropical land, including the maritime continent, most of which is beneficial compared to the Global Precipitation Climatology Project (GPCP, Adler et al. (2003)). Particularly relevant for the Maritime Continent, a significant issue noted by operational meteorologists with the control simulation in the tropics is precipitation in convective weather systems abruptly stopping at the coastline as they move from sea to land. This issue is much improved in CoMorph-A. Especially over the Pacific Ocean there is a sharpening of the ITCZ, giving enhanced rainfall on the equator with reductions to the north and south, with mixed impact.

More detailed analysis shows the characteristics of the model's tropical precipitation at local time and space scales are altered beyond recognition. Fig. 2 quantifies the probability of grid point precipitation rates at each timestep given the rate at the previous timestep. In the control model there is a strong signal along the axes, indicating a high probability of no precipitation on one timestep if there was precipitation on the previous, and vice versa – this illustrates the long-standing, Klingaman et al. (2017), time-step level intermittency in the control. With CoMorph-A this timestep intermittency is completely removed and shows a far more plausible temporal coherence with high probabilities around the one-to-one line. This continuity between time steps is a direct result of the use of improved numerical methods, as discussed in section 3, and the implicit solution for detrainment in CoMorph, in particular, as this will tend to maintain similar convective inhibition into the next time step. Interestingly, after averaging over 3 hours and 2x2 grid points for comparison with the GPM observations (Global Precipitation Measurement (GPM) Multi-satellitE Retrievals (IMERG) precipitation data V06B, Tan et al. (2019)), the models' precipitation characteristics are far more similar. This convergence is similar to that seen for a range of MetUM configurations at various resolutions in Martin et al. (2017) and similar to the results for a number of CMIP5 models (except for those with particularly coarse resolution) in Klingaman et al. (2017). There is, nevertheless, a suggestion of more temporally coherent heavy rain with CoMorph-A, closer to GPM, albeit still insufficient. It is also interesting to reflect that many of the geographical biases in tropical precipitation seen in Fig. 1 are remarkably similar, despite entirely replacing the convection scheme, although many of these simply reflect the regions with the heaviest rainfall.

The strength of propagating tropical waves is strongly improved, see Fig. 3, both for Kelvin waves (as marked on the figure) and the Madden-Julian Oscillation (MJO, the region of strong observed eastward-propagating 30–60 day variability at wave numbers 1 to 3). We believe this tighter coupling between CoMorph and the resolved dynamics arises because the initiation of massflux can respond to locally generated moist instability, but more detailed investigation will be the subject of future work.

Fig 4 shows a large increase in the integrated tropical water vapour that all but removes a dry bias in the control, largely occurring in the upper troposphere. Around a half of that moistening comes from the Fountain Buster scheme, while the rest is likely due to passing the precipitation into the "large-scale" microphysics that then represents its evaporation as it falls to the surface more realistically (although to confirm this would require adding some form of direct precipitation to the surface within CoMorph, which is beyond the scope of this work). This moister troposphere may also contribute to the improvement in the strength of tropical waves, see Fig. 3 (Zhu et al. (2023a)).

There are also substantial changes to the clouds in the model, as seen in the top-of-atmosphere cloud radiative effect (CRE, which is the clear-sky minus the total radiative flux). The longwave CRE, Fig. 5, is much stronger across the tropics and especially over tropical land, which all but eliminates a serious underestimate in the control. This is due to a large increase in the tropical ice cloud amount (both mass and cloud fraction) as can also be seen in the comparison with CALIPSO observations over central Africa in Fig. 6, likely arising from the handling of precipitation sedimentation by the grid-scale microphysics. However, like the control, there is less cloud than observed by CALIPSO between 5km and 8km altitude suggesting that the congestus phase remains poorly simulated. The increase in optically thick cirrus means shortwave CRE (Fig. 7) is also enhanced somewhat over tropical land, but the biggest impacts here are in the subtropics and especially over the eastern Pacific and Atlantic. Climatalogically, these are areas dominated by stratocumulus clouds. The geographical pattern of the change from including the CoMorph-A package matches remarkably well with the error in the control, although the end result is for the clouds to be somewhat too reflective over most of the tropical oceans. Part of the increase in stratocumulus arises from the implementation of BiModal initiation in the PC2 cloud scheme and the revised calculation of Ri, but around half comes from CoMorph itself, especially further west from the coastline where shallow cumulus clouds form under the lifting stratocumulus. Detailed single column model analysis of this transition region (not shown) indicates that the combination of the smoother temporal evolution of CoMorph (as in Fig 2) and more sensitive (implicit) detrainment allow a smoother evolution of the stratiform cloud layer as it rises away from the coast. Consistent with the improved top-of-atmosphere radiative fluxes, we also find the net surface energy fluxes (that are important for coupled ocean modelling) are significantly improved, and across the tropics and subtropics especially, compared to the observed estimate from Liu et al. (2015) (not shown).

A form of convective "memory" was implemented in the control model (in GA8GL9 relative to GA7GL7, as described in section 2) to delay the development of deep convection and help address the poor representation of the diurnal cycle of precipitation over land. However, consistent with other studies (Willett and Whitall (2017); Tao and et al (2024)), we find GA8GL9 still has issues in simulating the correct timing of the diurnal cycle over many areas of the globe (see Fig. 8). CoMorph-A does not have such a memory function and has a tendency to have the diurnal peak in rainfall intensity over tropical land around local noon or early afternoon, compared to the observed late evening peak (Fig. 8). Over some regions (e.g. Africa) this is earlier and hence detrimental compared with the control, whilst over others (e.g. S. E. Asia, as also seen in Zhu et al. (2023b)) CoMorph-A is an improvement on the control, although still considerably earlier than observed. Diurnal cycle experiments using the idealised MetUM (Lavender et al. (2024)) also show too early initiation and development to deep convection using CoMorph-A compared to high resolution simulations, although improved relative to the control.

5 | RESULTS IN NWP

The NWP trials (cycling forecasts and data assimilation) are performed at somewhat higher, N320 ($\sim$ 40 km in mid-latitudes), resolution than the climate simulations presented in section 4. A wide variety of metrics are monitored and these are summarised in the "scorecards" shown in Fig. 9. These illustrate the change in root-mean-square error (rmse) against each trial's own analysis (scorecards are also produced against observations and independent global analyses from ECMWF but those look very similar so are not shown). The majority of metrics show reductions in rmse with CoMorph-A, with somewhat better overall performance in the boreal summer than winter (overall reductions of 1.9% and 0.5% respectively). Some degradation is seen in a number of fields in the first two days that may arise from not updating the error covariance statistics in the trials. One field that shows degradation throughout the forecasts in both summer and winter, though, is the tropical temperature at 850 hPa. Fig. 10 shows the geographical distribution of the change in rmse at day 6, which has large positive values across most of the tropical oceans but especially so, for these austral summer trials, in the sub-tropical south-eastern Pacific and Atlantic close to the edges of where CoMorph-A gives more stratocumulus cloud layers (the NWP trials show a similar increase to that shown to be beneficial in the AMIP simulations in Fig. 7). Fig. 10 also shows that the standard deviation of temperature at 850 hPa in the analyses is increased in CoMorph-A, and the day 6 forecasts in CoMorph-A have similarly more variable temperatures at this level (not shown). The more persistent stratocumulus clouds with CoMorph-A will result in a sharper temperature inversion at the top of the boundary layer. Furthermore, on the western edge (and further downwind) of the stratocumulus, there is more variability of the cloud cover as it transitions to shallow cumulus. These transitions result in variations in the height of the inversion which will be manifested as increased temperature variability and rmse at this level, even if the average inversion height or boundary layer temperature were accurately forecast (the 1000 hPa temperature rmse is actually improved or neutral over tropical oceans, not shown).

A long standing systematic error is a slow bias in the winter extra-tropical jet. Fig. 11 shows an increase in the wind speed from CoMorph-A, reducing this error. It is often the case that increasing the wind speed will also increase the rmse due to a "double penalty" if a wind feature is geographically displaced. It is notable, therefore, that CoMorph-A reduces the slow bias with an overall neutral impact on rmse for upper level winds (Fig. 11 & Fig. 9).

Further analysis of the trials has included tracking the location of extra-tropical cyclones through the maximum in 850 hPa vorticity (Hodges (1995)). Whilst the error bars overlap and hence cannot be regarded as significantly different, the errors in these tracks are reduced in CoMorph-A and experience suggests the fact the signal is consistent in the two seasons is notable (Fig. 12).

Finally, between 25 June to 31 October 2021, atmosphere-only forecasts with the CoMorph-A package were run daily at the operational resolution of N1280 from Met Office operational analyses at 0 UTC. Verification of tropical cyclones from these forecasts in Fig. 13 shows CoMorph-A gave substantial deepening and improvement to wind speeds. Whilst the central pressure in these simulations is now lower than observed, they are atmosphere-only and we would expect slower-moving storms to be weaker when coupled to an ocean model in operational systems.

6 | CONCLUSIONS

The results from a range of global simulations have been presented for a large package of revised parametrization schemes, centred around the entirely new CoMorph massflux convection scheme. The key components of CoMorph are that it has a physically-based flexible formulation that allows it to represent all convective regimes and is tightly coupled to the rest of the model, both the other parametrization schemes and the dynamics. The main impacts of this overall CoMorph-A package in standard global test simulations are found to be:

- removal of the timestep level intermittency of convection that has been in all configurations of the MetUM since its inception
- improved tropospheric humidity over tropical land
- improved tropical variability, including Kelvin waves and MJO
- surface fluxes improved in many regions, important when coupling to an ocean model
- increased high cloud over tropical land where it has always been lacking and hence marks a significant improve-

ment

- increased low cloud over tropical oceans which is generally better but optically too bright everywhere (although tuned for the global mean net top-of-atmosphere radiative flux, in order to balance weak clear sky out-going longwave radiation)
- improved NWP performance, including reduced tropical and extra-tropical cyclone errors
- some degradation of the diurnal cycle of tropical precipitation

Given the extent of new developments within the CoMorph-A package, this represents impressive performance for a first implementation of a new convection scheme. Future work will focus on improving the diurnal cycle, through for example inclusion of a second updraught to represent, separately, convection forced from cold pools, and on CoMorph's applicability to higher resolutions, where the larger scales of convection begin to be resolved.

Acknowledgements

The contributions of A. P. Lock and M. Willett were supported by the Met Office Hadley Centre Climate Programme funded by DSIT. The contributions of M. Whitall, P. R. Field and G. Martin were supported by the Met Office Weather and Climate Science for Service Partnership (WCSSP) India, a collaborative initiative between the Met Office and the Indian Ministry of Earth Sciences (MoES). The contributions of M. Whitall, A. J. Stirling, K. D. Williams and M .Willett were supported by WCSSP Southeast Asia. The WCSSP programme is supported by the U.K. Government's Newton Fund. S. L. Lavender is funded through the Northern Australia Climate Program (NACP), funded by Meat and Livestock Australia, the Queensland Government through the Drought and Climate Adaptation Program, and the University of Southern Queensland. K. Matsubayashi was a visiting scientist working at the Met Office on secondment from the Japan Meteorological Agency under agreement number L4183. We also thank Duncan Ackerley for his help with the mid-latitude cyclone analysis. This work was carried out as part of the joint Met Office-NERC ParaCon programme (https://www.metoffice.gov.uk/research/approach/collaboration/paracon) and we are grateful to the ParaCon community for many stimulating discussions.

Data availability statement

The data that support the findings of this study are available from the corresponding author and Met Office co-authors upon reasonable request.

References

Adler, R. F., Huffman, G. J., Chang, A., Ferraro, R., Xie, P.-P., Janowiak, J., Rudolf, B., Schneider, U., Curtis, S., Bolvin, D., Gruber, A., Susskind, J., Arkin, P. and Nelkin, E. (2003) The version-2 global precipitation climatology project (gpcp) monthly precipitation analysis (1979–present). *J.Hydrometeor.*, **4**, 1147–1167.

Ahn, M.-S., Kim, D., Kang, D., Lee, J., Sperber, K. R., Gleckler, P. J. and et al (2020) Mjo propagation across the maritime continent: Are cmip6 models better than cmip5 models? *Geophysical Research Letters*, **47**.

Arakawa, A. and Schubert, W. H. (1974) Interaction of a cumulus cloud ensemble with the large-scale environment, part i. *J. Atmos. Sci.*, **31**, 674–701.

Bain, C. L., Williams, K. D., Milton, S. F. and Heming, J. T. (2014) Objective tracking of african easterly waves in met office models. *Q.J.R. Meteorol. Soc.*, **140**, 47–57.

Bush, M., Allen, T., Bain, C., Boutle, I., Edwards, J., Finnenkoetter, A., Franklin, C., Hanley, K., Lean, H., Lock, A., Manners, J., Mittermaier, M., Morcrette, C., North, R., Petch, J., Short, C., Vosper, S., Walters, D., Webster, S., Weeks, M., Wilkinson, J., Wood, N., and Zerroukat, M. (2020) The first met office unified model–jules regional atmosphere and land configuration, ral1. *Geosci. Model Dev.*, **13**, 1999–2029.

Christopoulos, C. and Schneider, T. (2021) Assessing biases and climate implications of the diurnal precipitation cycle in climate models. *Geophysical Research Letters*, **48**.

Daleu, C. L., Plant, R. S., AJ, S. and Whitall, M. (2023) Evaluating the comorph parameterization using idealised simulations of the two-way coupling between convection and large-scale dynamics. *Quart. J. Royal Meteorol. Soc.*, **149**, 3087–13109.

Derbyshire, S., Maidens, A., Milton, S. F., Stratton, R. A. and Willett, M. R. (2011) Adaptive detrainment in a convective parametrization. *Q.J.R. Meteorol. Soc.*, **137**, 1856–1871.

Dias, J., Gehne, M., Kiladis, G. and Magnusson, L. (2023) The role of convectively coupled equatorial waves in sub-seasonal predictions. *GRL*, **50**.

Edwards, J. and Slingo, A. (1996) Studies with a flexible new radiation code. i: Choosing a configuration for a large-scale model. *Q.J.R. Meteorol. Soc.*, **122**, 689– 719.

Fletcher, J. and Bretherton, C. (2010) Evaluating boundary layer–based mass flux closures using cloud-resolving model simulations of deep convection. *J. Atmos. Sci.*, **67**, 2212–2225.

Furtado, K. and Field, P. (2017) The role of ice-microphysics parametrizations in determining the prevalence of supercooled liquid water in high-resolution simulations of a southern ocean midlatitude cyclone. *Journal of the Atmospheric Sciences*, **74**, 2001–2021.

Gregory, D. and Rowntree, P. R. (1990) A mass flux convection scheme with representation of cloud ensemble characteristics and stability-dependent closure. *Mon. Wea. Rev.*, **118**, 1483–1506.

Hanley, K., Whitall, M., Stirling, A. and Clark, P. (2019) Modifications to the representation of subgrid mixing in kilometre-scale versions of the unified model. *Q. J. Roy. Meteorol. Soc.*, **145**, 3361–3375.

Hill, P. G., Morcrette, C. J. and Boutle, I. A. (2015) A regime-dependent parametrization of subgrid-scale cloud water content variability. *Q. J. Roy. Meteorol. Soc.*, **141**, 1975–1986.

Hodges, K. I. (1995) Feature tracking on the unit sphere. *Mon. Wea. Rev.*, **123**, 3458–3465.

Holloway, C., Petch, J., Beare, R., Bechtold, P., Craig, G., S.H., D., Donner, L., Field, P., Gray, S., Marsham, J., Parker, D., Plant, R., Roberts, N., Schultz, D., Stirling, A. and Woolnough, S. (2014) Understanding and representing atmospheric convection across scales: recommendations from the meeting held at dartington hall, devon, uk, 28–30 january 2013. *Atmospheric Science Letters*, **14**, 348–353.

Huffman, G. J., Adler, R. F., Bolvin, D. T., Gu, G., Nelkin, E. J., Bowman, K., Stocker, E. and Wolff, D. (2007) The trmm multi-satellite precipitation analysis (tmpa): quasi-global, multiyear, combined-sensor precipitation estimates at fine scales. *J. Hydrometeorol.*, **8**, 38–55.

Janiga, M. A. C. J. S., Ridout, J. A., Flatau, M., Barton, N. P., Metzger, E. J. and Reynolds, C. A. (2018) Subseasonal forecasts of convectively coupled equatorial waves and the mjo: Activity and predictive skill. *Mon. Wea. Rev.*, **146**, 2337–2360.

Kershaw, R. and Cregory, D. (1997) Parametrization of momentum transports by convection. i: Theory and cloud modelling results. *Q. J. R. Meteorol. Soc.*, **123**, 1133–1151.

Klingaman, N. P., Martin, G. M. and Moise, A. (2017) Asop (v1.0): a set of methods for analyzing scales of precipitation in general circulation models. *Geosci. Model Dev.*, **10**, 57–83.

Klingaman, N. P. and Woolhough, S. J. (2013) Using a case-study approach to improve the madden–julian oscillation in the hadley centre model. *Quart. J. Royal Meteorol. Soc.*, **140**, 2491–2505.

Lavender, S. L., Stirling, A. J., Whitall, M., Stratton, R., Daleu, C. L., Plant, R. S. and Lock, A. (2024) The use of idealised experiments in testing a new convective parameterization: Performance of comorph-A. *Accepted for Quart. J. Royal Meteorol. Soc.*

Liu, C., Allan, R., Berrisford, P., Mayer, M., Hyder, P., Loeb, N., Smith, D., Vidale, P.-L. and Edwards, J. (2015) Combining satellite observations and reanalysis energy transports to estimate global net surface energy fluxes 1985–2012. *JGR Atmospheres*, **120**.

Liu, Y., Daum, P. H., Guo, H. and Peng, Y. (2008) Dispersion bias, dispersion effect, and the aerosol–cloud conundrum. *Environ. Res. Lett.*, **3**.

Lock, A., Brown, A., Bush, M., Martin, G. and Smith, R. (2000) A new boundary layer mixing scheme. part i: Scheme description and single-column model tests. *Monthly Weather Review*, **128(9)**, 3187–3199.

Loeb, N., Wielicki, B. A., Wong, T. and Parker, P. A. (2009) Impact of data gaps on satellite broadband radiation records. *J. Geophys. Res. Atmos.*, **114**.

Manners, J., Edwards, J. M., Hill, P. and Thelen, J.-C. (2015) Socrates (suite of community radiative transfer codes based on edwards and slingo) technical guide. *Met Office, UK*.

Mapes, B. (2000) Convective inhibition, subgrid-scale triggering energy, and stratiform instability in a toy tropical wave model. *J. Atmos. Sci*, **57**.

Mapes, B. and Neale, R. (2011) Parameterizing convective organization to escape the entrainment dilemma. *Journal of Advances in Modeling Earth Systems*, **3**.

Martin, G. M., Klingaman, N. P. and Moise, A. (2017) Connecting spatial and temporal scales of tropical precipitation in observations and the metum-ga6. *Geosci. Model Dev.*, **10**, 105–126.

Morcrette, C. (2012) Improvements to a prognostic cloud scheme through changes to its cloud erosion parametrization. *Atmospheric Science Letters*, **13**, 95–102.

— (2020) Modification of the thermodynamic variability closure in the met office unified model prognostic cloud scheme. *Atmospheric Science Letters*, **22**.

Mulcahy, J. P., Jones, C., Sellar, A., Johnson, B., Boutle, I. A., Jones, A., Andrews, T., Rumbold, S. T., Mollard, J., Bellouin, N., Johnson, C. E., Williams, K. D., Grosvenor, D. P. and T., M. D. (2018) Improved aerosol processes and effective radiative forcing in hadgem3 and ukesm1. *Journal of Advances in Modeling Earth Systems*, **10**.

Sherwood, S., Bony, S. and Dufresne, J. (2014) Spread in model climate sensitivity traced to atmospheric convective mixing. *Nature*, **505**, 37–42.

Tan, J., Huffman, G. J., Bolvin, D. T. and J., N. E. (2019) Diurnal cycle of imerg v06 precipitation. *Geophys. Res. Lett.*, **46**, 13584–13592.

Tao, C. and et al (2024) Diurnal cycle of precipitation over the tropics and central united states: intercomparison of general circulation models. *Quart. J. Royal Meteorol. Soc.*, 1–26.

Tomassini, L. (2018) Mesoscale circulations and organized convection in african easterly waves. *J. Atmos. Sci.*, **75**, 4357–4381.

Uppala, S. M., KAllberg, P. W., J, S. A. and et al (2005) The era-40 re-analysis. *Q. J. Roy. Meteorol. Soc.*, **131**, 2961–3012.

Van Weverberg, K., Boutle, I., Morcrette, C. and Newsom, R. (2016) Towards retrieving critical relative humidity from ground-based remote-sensing observations. *Quart. J. Royal Meteorol. Soc.*, **142**, 2867–2881.

Vitart, F., Woolnough, S., Balmaseda, M. A. and Tompkins, A. M. (2007) Monthly forecast of the madden–julian oscillation using a coupled gcm. *Mon. Weather Rev.*, **135**, 2700—-2715.

Walters, D., Baran, A., Boutle, I., Brooks, M., Earnshaw, P., Edwards, J., Furtado, K., Hill, P., Lock, A., Manners, J., Morcrette, C., Mulcahy, J., Sanchez, C., Smith, C., Stratton, R., Tennant, W., Tomassini, L., van Weverberg, K., Vosper, S., Willett, M., Browse, J., Bushell, A., Carslaw, K., Dalvi, M., Essery, R., Gedney, N., Hardiman, S., Johnson, B., Johnson, C., Jones, A., Jones, C., Mann, G., Milton, S., Rumbold, H., Sellar, A., Ujiie, M., Whitall, M., Williams, K. and Zerroukat, M. (2019) The met office unified model global atmosphere 7.0/7.1 and jules global land 7.0 configurations. *Geosci. Model Dev.*, **12**, 1909–1963.

Weverberg, K. V., Morcrette, C. J., Boutle, I., Furtado, K. and Field, P. R. (2021) A bimodal diagnostic cloud fraction parameterization. part i: Motivating analysis and scheme description. *Mon. Weather Rev.*, **149**, 841–857.

Whitall, M., Stirling, A., Lavender, S., Stratton, R. and Matsubayashi, K. (2022) The comorph convection scheme. um documentation paper 043. *Technical report no. 617, Met Office*.

Willett, M. and Whitall, M. (2017) A simple prognostic based convective entrainment rate for the unified model: Description and tests. *Met Office*.

Williams, K. D., van Niekerk, A., Best, M. J., Lock, A. P., Brooke, J. K., Carvalho, M. J., Derbyshire, S. H., Dunstan, T. D., Rumbold, H. S., Sandu, I. and Sexton, D. M. H. (2020) Addressing the causes of large-scale circulation error in the met office unified model. *Q. J. Roy. Meteorol. Soc.*, **146**, 2597–2613.

Wilson, D. R. and Ballard, S. P. (1999) A microphysically based precipitation scheme for the uk meteorological office unified model. *Q. J. Roy. Meteorol. Soc.*, **125**, 1607–1636.

Wilson, D. R., Bushell, A. C., Kerr-Munslow, A. M., Price, J. D. and Morcrette, C. J. (2008a) Pc2: A prognostic cloud fraction and condensation scheme. i: Scheme description. *Q. J. Roy. Meteorol. Soc.*, **134**, 2093–2107.

Wilson, D. R., Bushell, A. C., Kerr-Munslow, A. M., Price, J. D., Morcrette, C. J. and Bodas-Salcedo, A. (2008b) Pc2: A prognostic cloud fraction and condensation scheme. i: Climate model simulations. *Q. J. Roy. Meteorol. Soc.*, **134**, 2109–2125.

Winker, D. M., Pelon, J. and McCormick, M. P. (2002) The calipso mission: Spaceborne lidar for observation of aerosols and clouds. *Proc. SPIE*, **4893**, 1–11.

Wood, N., Staniforth, A., White, A., Allen, T., Diamantakis, M., Gross, M., Melvin, T., Smith, C., Vosper, S., Zerroukat, M. and Thuburn, J. (1999) An inherently mass-conserving semi-implicit semi-lagrangian discretization of the deep-atmosphere global non-hydrostatic equations. *Q. J. Roy. Meteorol. Soc.*, **140**, 1505–1520.

Xie, S.and Ma, H., Boyle, J., Klein, S. and Zhang, Y. (2012) On the correspondence between short- and long-time-scale systematic errors in cam4/cam5 for the year of tropical convection. *J. Climate*, **25**, 7937–7955.

Yang, G.-Y. and Slingo, J. (2001) The diurnal cycle in the tropics. *Mon. Weather Rev.*, **129**, 784–801.

Zhu, H., H., H. and C., J. (2023a) Convection in a parameterized and super-parameterized model and its role in the representation of the mjo. *J. Atmos. Sci.*, **66**, 2796–2811.

Zhu, H., Hudson, D., Li, C., Shi, L., Young, G., Stirling, A., Whitall, M., Lock, A., Lavender, S. and Stratton, R. (2023b) Impacts of the new um convection scheme, comorph-a, over the indo-pacific and australian regions. *Submitted to Journal of Southern Hemisphere Earth Systems Science*.

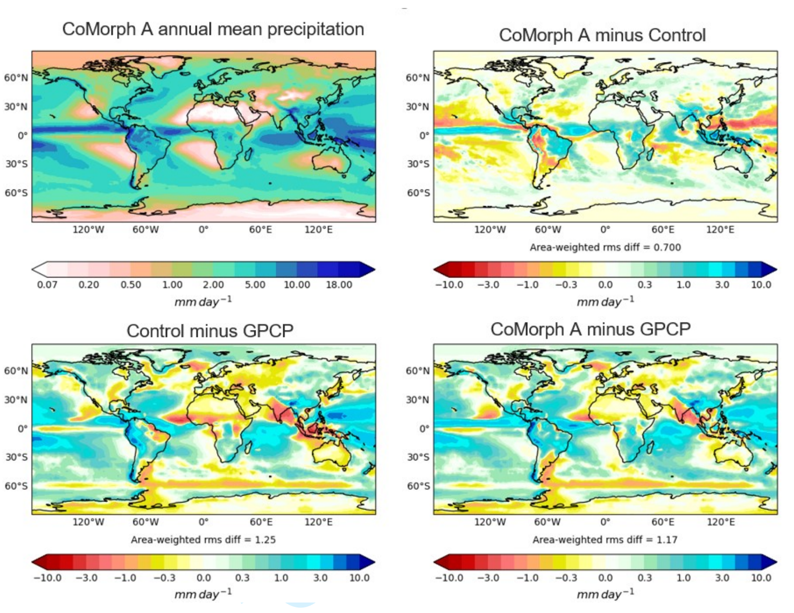

FIGURE 1 Annual mean precipitation biases compared to GPCP observations from N96 AMIP simulations

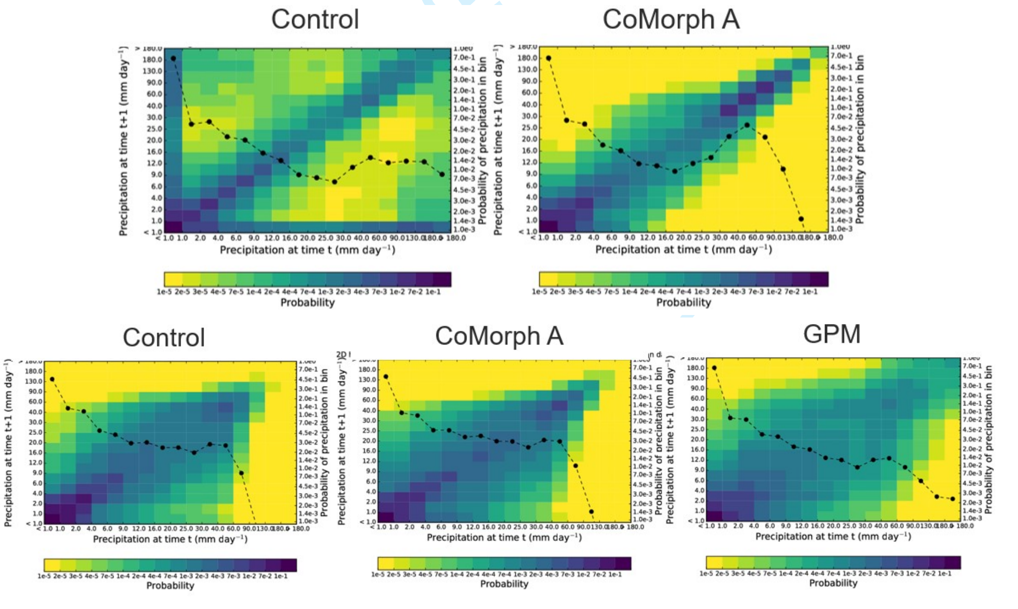

FIGURE 2 Histograms of the probability of bins of precipitation, measured at the time step and grid point level (top row) and over 3 hourly and 2x2 grid box averages (bottom row), aggregated over all grid points in the equatorial Indian Ocean from N96 AMIP simulations. The dashed lines show the one-dimensional histogram of the binned precipitation, using the right-hand vertical axis.

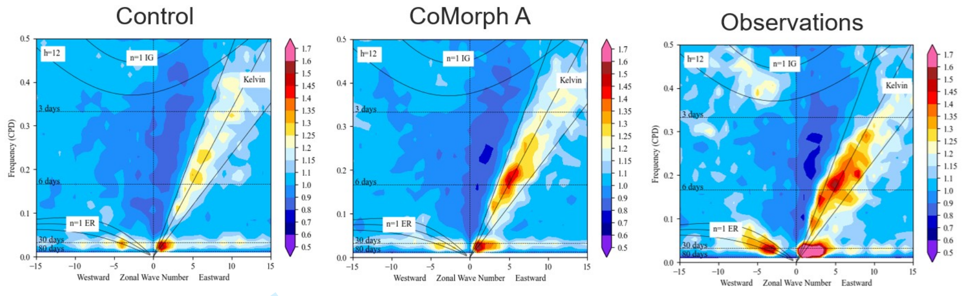

FIGURE 3 Wavenumber – frequency spectra of symmetric component of precipitation divided by the background power from N96 AMIP simulation. The observations are from TRMM 3B42 (Huffman et al. (2007))

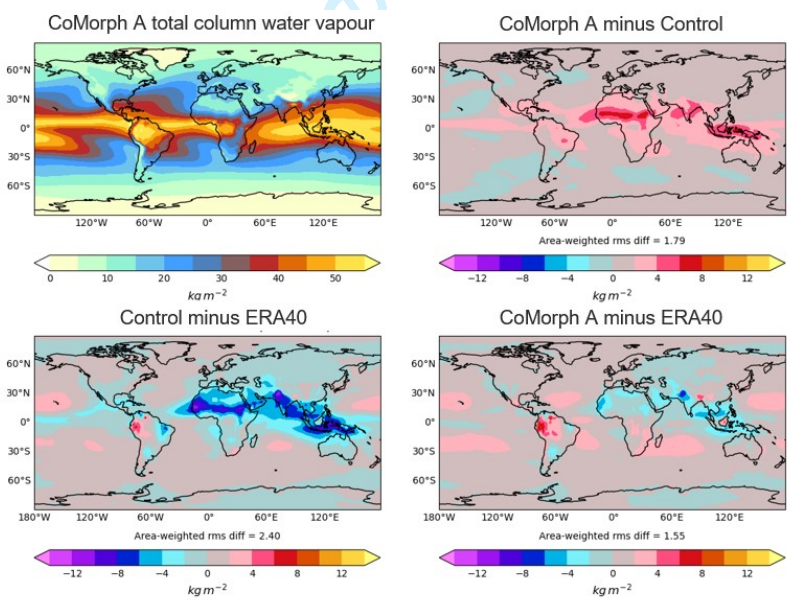

FIGURE 4 Annual mean total column water vapour from N96 AMIP simulations, and compared to ERA40 (Uppala et al. (2005)) in the bottom row.

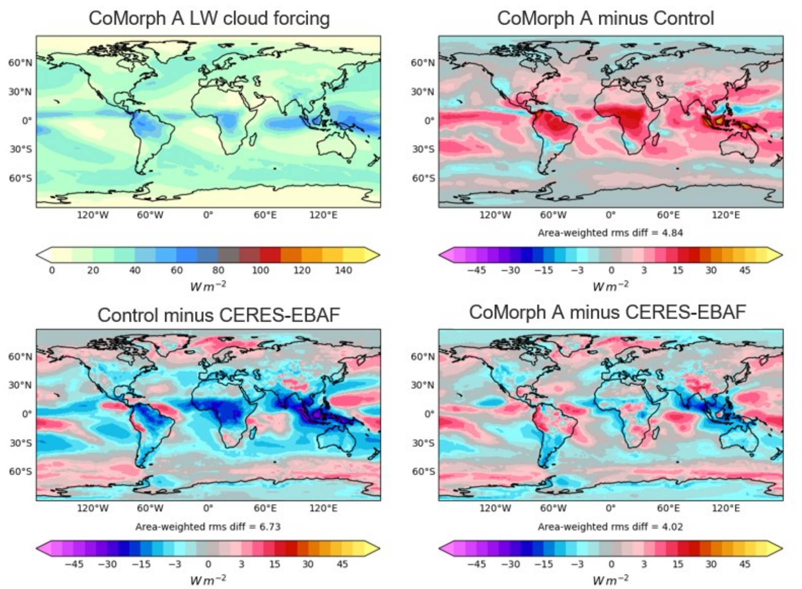

FIGURE 5 Longwave cloud radiative effect compared to Clouds and the Earth's Radiant Energy System (CERES) Energy Balanced and Filled (EBAF) dataset (Loeb et al. (2009)) from N96 AMIP simulations

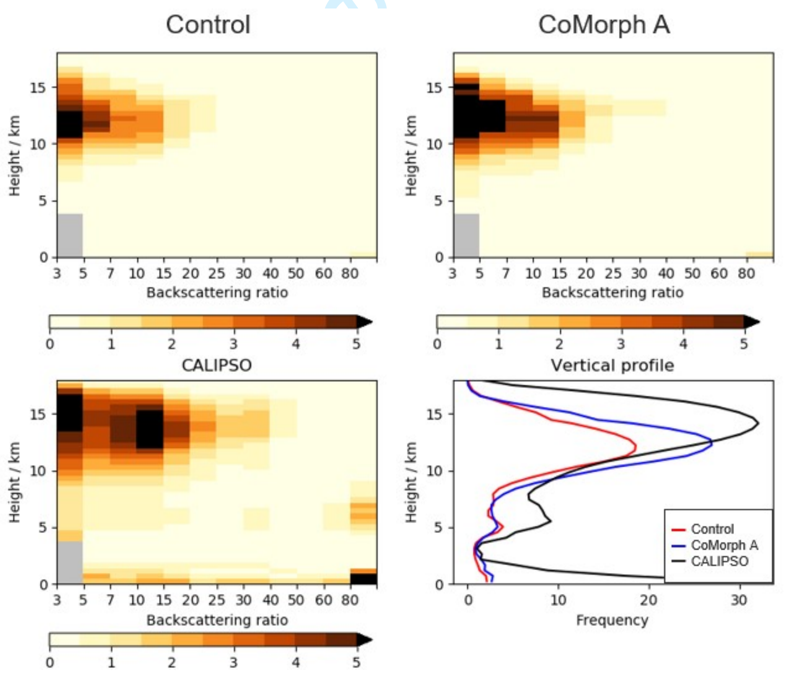

FIGURE 6 Histograms of height vs 532nm lidar backscatter ratio over central Africa (15^{o}E-30^{o}E, 20^{o}S-10^{o}N), showing climatologies of CALIPSO observations (Winker et al. (2002)) and simulated climatologies of CALIPSO data from 20-year N96 atmosphere/land-only climate simulations from the control and CoMorph-A

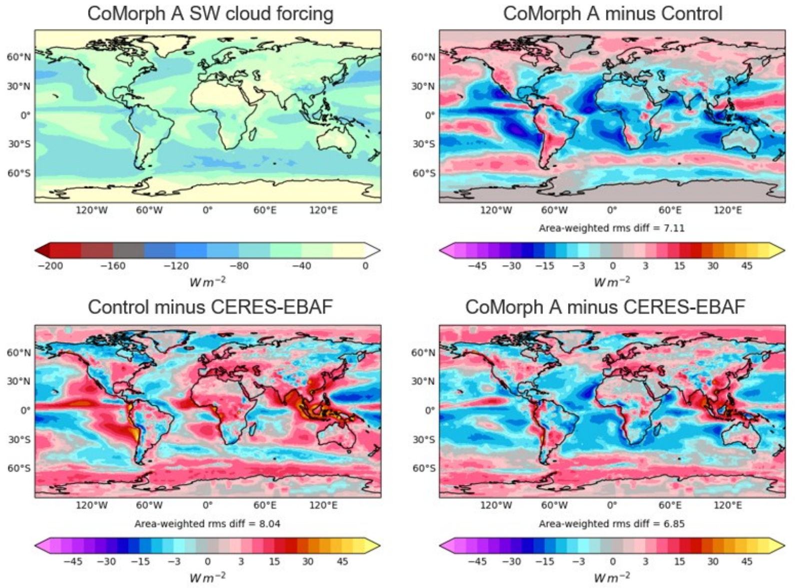

FIGURE 7 Shortwave cloud radiative effect compared to CERES-EBAF from N96 AMIP simulations

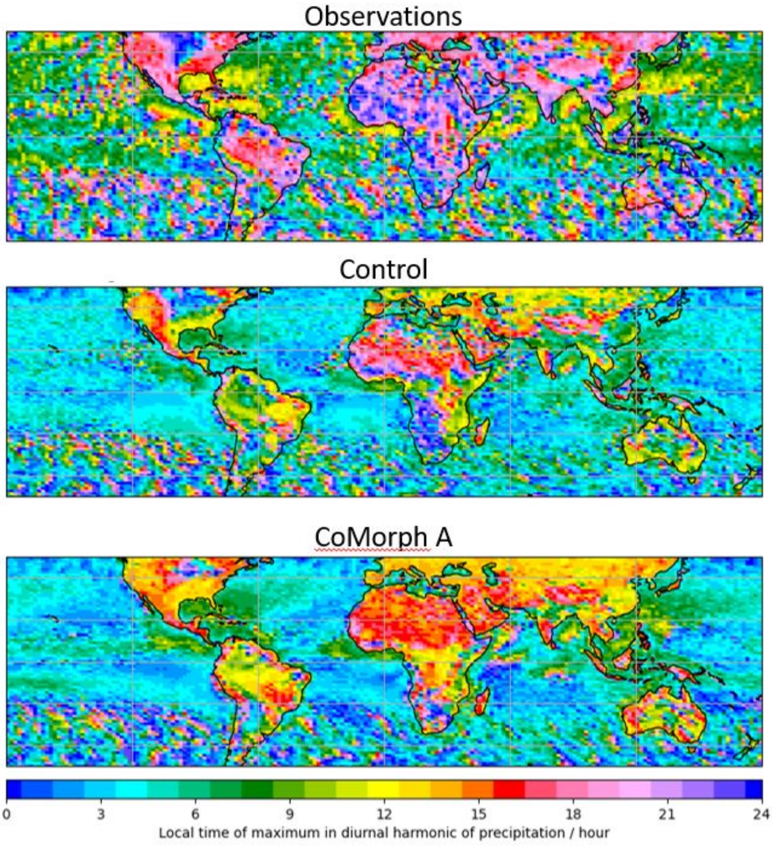

FIGURE 8 Local time of maximum in the diurnal harmonic of precipitation during JJA compared to TRMM 3B42 observations

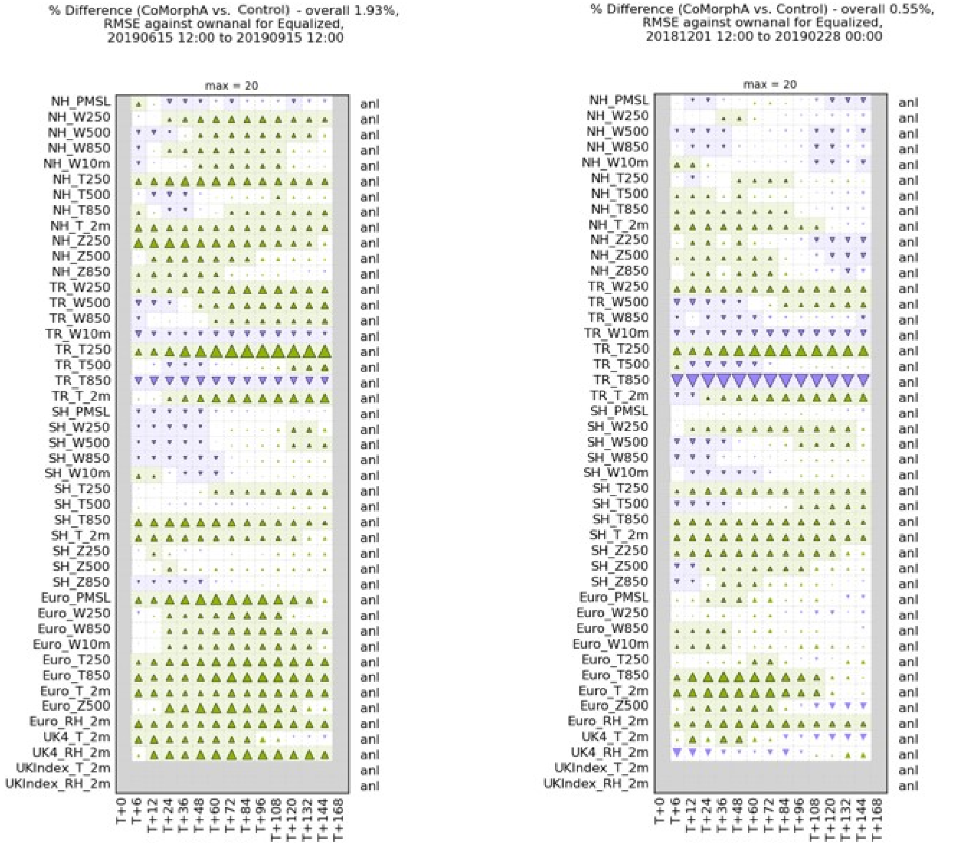

FIGURE 9 Scorecards against own analysis from the summer (left) and winter (right) NWP trials. Green upward triangles indicate reductions in root-mean-square error (rmse) and purple downward triangles increases, with the size of each scaled by the magnitude of change. Parameters are evaluated in the Northern Hemisphere (NH, north of 18.75° N), the tropics (TR, within 18.75° of the equator), the Southern Hemisphere (SH, south of 18.75° S), Europe (Euro) and UK (UK4 and UKIndex). The parameters are pressure at mean sea level (PMSL), vector wind (W), temperature (T) and geopotential height (Z) at various pressure levels given in hectopascals (such that NH_T250, for example, measures the change in rmse temperatures at 250 hPa in the northern hemisphere region). The columns represent forecast ranges from 6 h (T+6) to 7 days (T+168).

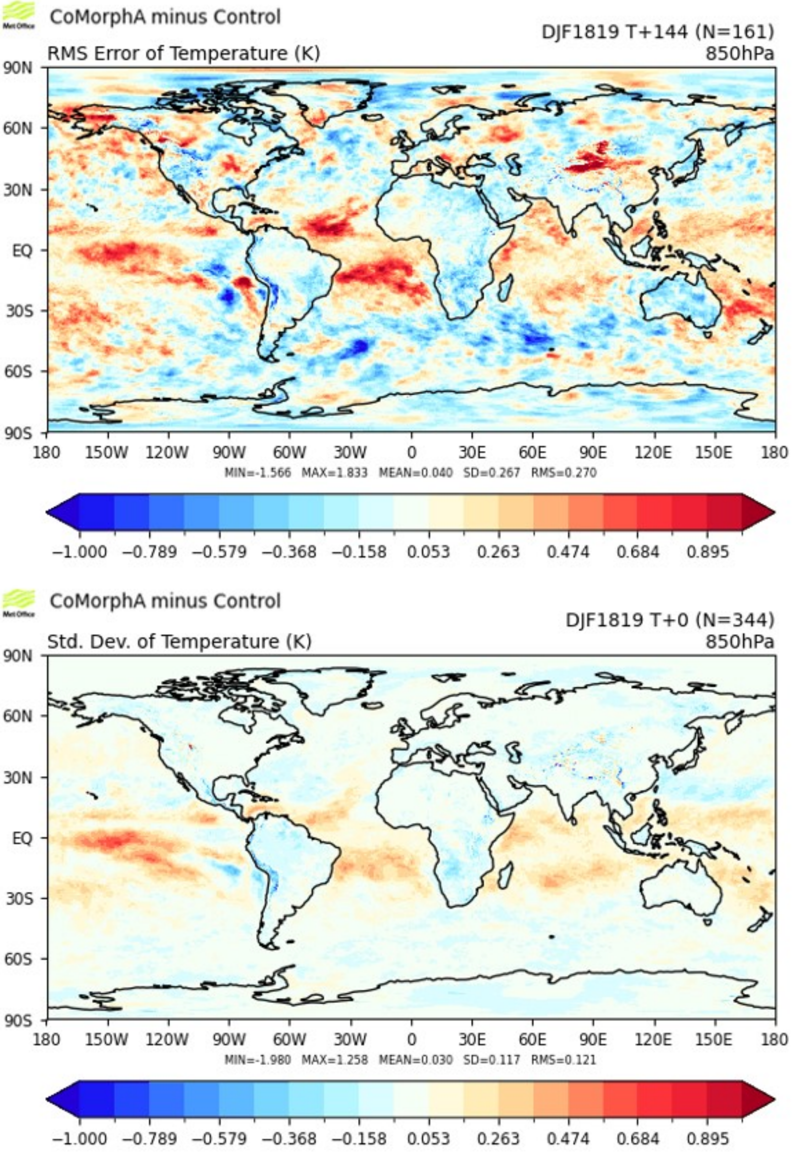

FIGURE 10 Change in root-mean-square error against own analysis of day 6 temperature at 850 hPa (top) and change in standard deviation of the analyses (bottom), from the winter NWP trials

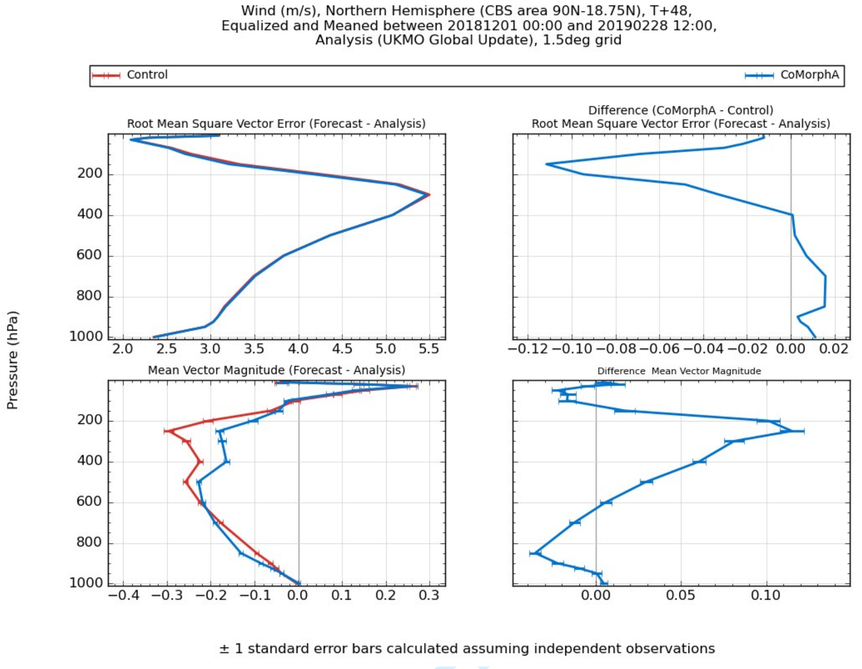

FIGURE 11 Profile of root mean square error (top left) and bias (bottom right) for northern hemisphere wind at T+48 of the DJF trial.

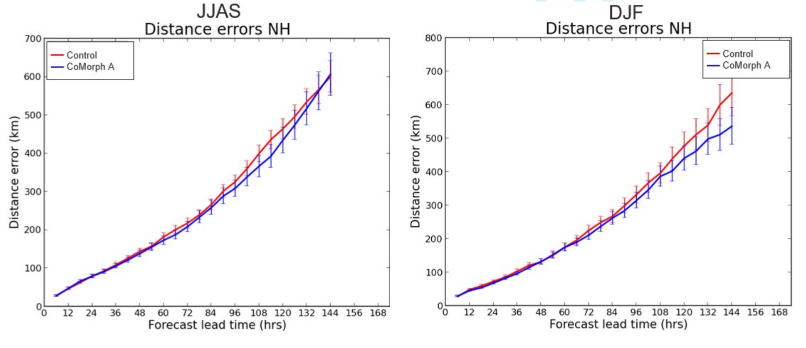

FIGURE 12 Extratropical cyclone track errors from the summer (left) and winter (right) NWP trials

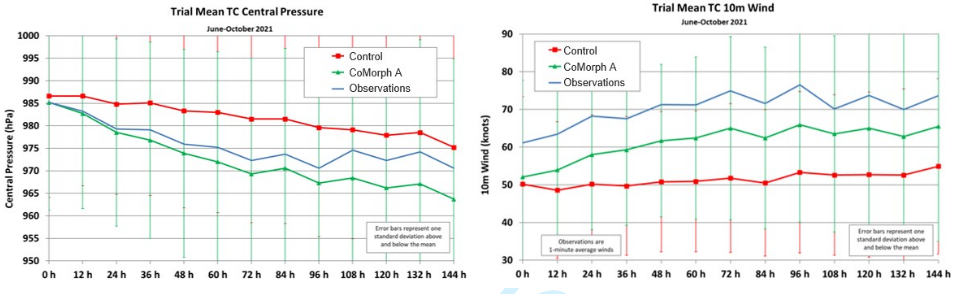

FIGURE 13 Tropical cyclone verification from the control and CoMorph-A forecasts at N1280 from June to October 2021

ORIGINAL ARTICLE
Journal Section

The performance of the CoMorph-A convection package in global simulations with the Met Office Unified Model

A. P. Lock[1] | M. Whitall[1] | A. J. Stirling[1] | K. D. Williams[1] | S. L. Lavender[2,1] | C. Morcrette[1] | K. Matsubayashi[3] | P. R. Field[1] | G. Martin[1] | M. Willett[1] | J. Heming[1]

[1]Met Office, FitzRoy Way, Exeter, EX1 3PB.

[2]Centre for Applied Climate Sciences, University of Southern Queensland, Toowoomba, Australia.

[3]Japan Meteorological Agency, Minato City, Tokyo, Japan

Correspondence
Met Office, FitzRoy Way, Exeter, EX1 3PB.
Email: adrian.lock@metoffice.gov.uk

Funding information

The impact on global simulations of a new package of physical parametrizations in the Met Office Unified Model is documented. The main component of the package is an entirely new convection scheme, CoMorph. This has a mass-flux structure that allows initiation of buoyant ascent from any level and the ability for plumes of differing originating levels to coexist in a grid box. it has a different form of closure, where the mass-flux of initiation is dependent on local instability, and an implicit numerical solution for detrainment that yields smooth timestep behaviour. The scheme is more consistently coupled to the cloud, microphysics and boundary layer parametrizations and, as a result, significant changes to these have also been made. The package, called CoMorph-A, has been tested in a variety of single-column and idealised regimes. Here we test it in global configurations and evaluate it against observations using a range of standard metrics. Overall it is found to perform well against the control. Biases in the climatologies of the radiative fluxes are significantly reduced across the tropics and sub-tropics, tropical and extratropical cyclone statistics are improved and the MJO and other propagating tropical waves are strengthened. It also improves overall scores in NWP trials, without revisions to the data assimilation. There is still work to do to improve the diurnal cycle of precipitation over land, where the peak remains too close to the middle of the day.

KEYWORDS
Convection, parametrization, global, evaluation, Unified Model

1 | INTRODUCTION

The representation of convection in general circulation models (GCMs) has long been recognised as having a central control on model performance, not only influencing the distribution of precipitation, but also global circulation patterns, and the resulting cloud and radiative fluxes that respond to them (e.g. Xie et al. (2012), Holloway et al. (2014) and Sherwood et al. (2014)). Common to many GCMs, the Unified Model has previously used a mass-flux scheme based on simplified Arakawa-Schubert principles (Arakawa and Schubert (1974)), which was devised by Gregory and Rowntree (1990), and used largely predefined profiles for entrainment, a simple link to detrainment, along with a CAPE-based closure. While this scheme and its subsequent variants (e.g. Derbyshire et al. (2011), Walters et al. (2019), Willett and Whitall (2017)) has been able to produce good mean atmospheric states (e.g. Walters et al. (2019)), it has had difficulty generating appropriate coupling between convection and the model dynamics. This is seen in a range of emergent atmospheric phenomena that rely on the close feedbacks between convection and the larger-scale dynamics. Examples, in the UM and many other GCMs, include the insufficient strength and progression of the MJO, (e.g. Klingaman and Woolhough (2013) and Ahn et al. (2020)); the low amplitude of convectively-coupled Kelvin and other equatorial waves (Vitart et al. (2007), Janiga et al. (2018) and Dias et al. (2023)); the limited strength and frequency of African Easterly waves (Bain et al. (2014)), and their link to mesoscale convective systems (Tomassini (2018)). At the heart of the difficulty in representing these phenomena (in the current and earlier generations of GCM resolutions), lies the need to enable appropriate positive feedbacks to develop between convection and its parent dynamics, while keeping the model stable by preventing the emergence of convective instability onto the resolved grid.

The need for model stability has similarly made an apparently straightforward problem of capturing the correct timing (and amplitude) of the diurnal cycle of convection over land (Yang and Slingo (2001), Christopoulos and Schneider (2021), and Tao and et al (2024)) a challenge to rectify, as delaying convective activity for too long in the presence of a convectively-unstable atmosphere risks instability reaching the scale of the model grid, and the resolved dynamics responding accordingly.

Mass-flux schemes that use a closure based on convective available potential energy (CAPE) have success in keeping the resolved model stable (e.g. Walters et al. (2019)), but the use of such a vertical integral of convective instability in the troposphere to determine the mass flux at cloud base produces a disconnection between the conditions required in the boundary layer to trigger convection (for example, enough kinetic energy to overcome layers of convective inhibition), and those linked to its response (e.g.Mapes (2000) and Fletcher and Bretherton (2010). This can lead to numerical intermittency of CAPE-closed schemes across the timestep, as the CAPE-closure can create enough convective inhibition to prevent triggering on the next timestep (e.g. Klingaman et al. (2017)). Furthermore closures based on CAPE desensitise convective activity to local variations in the vertical thermodynamic profile, making it harder for the convection scheme to respond in tandem with the resolved dynamics (Whitall et al. (2022)). In addition, the use of predefined profiles for entrainment leads to somewhat inflexible representations of the mass-flux shape, making smooth transitions between different convective states hard to achieve.

These limitations, along with embedded decisions in the convection-scheme code about the levels of convective initiation, and the number of updraughts allowed at any one level, have motivated the development of an entirely new convection scheme called CoMorph, Whitall et al. (2022). This scheme provides a much more flexible architecture that enables complexity to be built in as required, and with the aim of creating a scheme that is better connected to the underpinning physical processes that drive convective activity.

CoMorph-A represents a first implementation of this scheme, designed for a global package, with the priorities of this version being to improve the coupling between convection and the resolved dynamics, as well as the consistency of interaction with other physics parametrisations. Numerous tests of the scheme under controlled forcing conditions have been conducted, for example in a Single Column Model (Whitall et al. (2022)), and for a range of case studies in the Idealised MetUM (a 3D, Cartesian, bi-periodic version of the Met Office Unified Model, Lavender et al. (2024)), with promising behaviour across a range of regimes. The coupling of the scheme to the dynamics has also been investigated (Daleu et al. (2023)), again highlighting the significant advances and potential of the new scheme. Zhu et al. (2023b) have also investigated the impacts of CoMorph-A in global simulations, focusing on the Indo-Pacific and Australian regions, finding significant benefits.

This paper introduces the CoMorph-A and accompanying control package configurations of the Met Office Unified Model (UM) in sections 2 and 3. To evaluate the impacts and performance of the new package, we follow the standard testing procedure as laid out in Walters et al. (2019), and evaluate the performance of the same configuration in both climate and numerical weather prediction (NWP). The climate evaluation in section 4 uses 20 years of simulation using AMIP specified sea-surface temperatures and sea ice. For NWP, while we have also run forecast only simulations, as in Walters et al. (2019), in section 5 we present verification from two 3-month long cycling forecast and analysis trials of the CoMorph-A package, so including 4DVar data assimilation (albeit without updating the error covariance and other assimilation statistics).

2 | CONTROL MODEL

The control configuration of the Met Office Unified Model (MetUM) used in this study is GA8GL9, which is based on ~~GAL7.1~~GA7GL7 (Walters et al. (2019)) but incorporates new~~the~~ developments ~~that were already~~ intended for the next release ~~and~~that will be documented in detail elsewhere. ~~That new trunk configuration, GAL8,~~GA8GL9 is the basis for the current operational NWP at the Met Office at the time of writing. The main changes since ~~GAL7.1~~GA7GL7 are:

- a package of changes related to model drag, described in Williams et al. (2020)
- revised parametrizations in the grid-scale microphysics for riming and the depositional growth of ice (Furtado and Field (2017))
- a new "multigrid" dynamical solver
- reduced drag at high wind speeds over the sea which improves forecasts of tropical cyclones at higher model resolutions than discussed here
- significant modifications to the existing massflux convection scheme

To give a brief description of ~~GAL7.1~~GA7GL7, the ENDGame dynamical core uses a semi-implicit semi-Lagrangian formulation to solve the non-hydrostatic, fully compressible deep-atmosphere equations of motion (Wood et al. (1999)). The grid-scale microphysics scheme (i.e., that which operates on the gridded prognostic variables) is single-moment with prognostic rain and ice, based on Wilson and Ballard (1999). The parametrisation of the fraction of the grid box which is covered by cloud, and the amount and phase of condensed cloud water it contains, is the prognostic cloud fraction and prognostic condensate (PC2) scheme (Wilson et al. (2008a), Wilson et al. (2008b)). The parametrization of radiative transfer (solar, shortwave (SW), and thermal, longwave (LW)) uses the SOCRATES scheme (Edwards and Slingo (1996); Manners et al. (2015) The turbulence scheme uses a first-order closure from Lock et al. (2000), mixing adiabatically conserved heat and moisture variables, momentum and tracers, using non-local profiles of diffusion coefficients within convective boundary layers and an explicit parametrization of entrainment across their top. In the control simulations the parametrization of sub-grid-scale transport of heat, moisture and momentum associated with cumulus clouds is a mass-flux convection scheme based on Gregory and Rowntree (1990). Three separate classes of convection are represented. First a diagnosis is made to determine whether convection is possible from the boundary layer, and its potential depth, using an adiabatic undilute parcel ascent, which then triggers either a shallow or deep convection scheme. Any remaining instability to moist ascent identified above the boundary layer and the top of any shallow or deep convection is handled by a mid-level scheme. Each component involves different parametrization of processes such as entrainment and detrainment from the plume, together with separate closures (based on the surface buoyancy flux for shallow convection and CAPE for mid-level and deep).

Of the modifications to the ~~GAL7.1~~GA7GL7 convection scheme used in our control, two are of most relevance here. The first, described in Willett and Whitall (2017), is to relate the entrainment rate in the deep component of the scheme to the amount of recent convective activity, as measured by an advected prognostic, similar to Mapes and Neale (2011). The source term for this is scaled on the surface convective precipitation rate, expanded to three dimensions using the current convective temperature increment profile, and decays with a 3 hour timescale. In this way the scheme is given a short term memory of previous convective activity, thereby allowing evolution of convective clouds over finite time scales. The second significant change from ~~GAL7.1~~GA7GL7 is to time-smooth the heat and moisture increments from the convection scheme over a timescale of 45 minutes. This is to reduce the impact of strong time-step-level intermittency in the scheme (see section 4) on the resolved scale dynamics. Note that this increment smoothing is *not* used with the CoMorph-A package.

Finally, note that most of these parametrizations have undergone significant modification between their original references, as above, and ~~GAL7.1~~GA7GL7 and the reader is referred to Walters et al. (2019) for more detail.

3 | COMORPH-A PACKAGE

An important aspect of the new convection parametrization, CoMorph, is that it is directly coupled to, and hence strongly dependent on, other aspects of the model physics. In particular, the presence or otherwise of cloud strongly affects the initial sources of mass, and the turbulence statistics from the boundary layer scheme determine the initial characteristics of the plume. Initial development in a single-column version of the MetUM highlighted unwanted sources of intermittency and sporadic unrealistic behaviour at the time step and grid level. For the proper functioning of the CoMorph convection scheme, as well as for the overall performance, it was therefore necessary to make significant changes to several other aspects of the physical parametrizations that will be described in this section. Together these then form the CoMorph-A package.

3.1 | CoMorph convection scheme

The control convection scheme is replaced by the entirely new scheme, CoMorph. Details are given in Whitall et al. (2022) but we give a summary here.

As in the control, the CoMorph scheme uses the massflux approach to parametrize the effects of subgrid cumulus convection but CoMorph has an entirely new code structure, to allow greater flexibility, and many differences in approach with additional physical processes included. There is no external closure in CoMorph. Instead, the massflux initiated from any locally unstable model grid-level is proportional to the relative size of the local environment lapse rate to that of a test parcel. Where the prognostic cloud fraction parametrization identifies a grid box as having partial cloud cover, separate initiation calculations are made in the saturated and unsaturated air and these are combined using area weighting by the cloud fraction.

The rate of entrainment scales with an inverse parcel radius, i.e.,

$$\epsilon = \frac{\alpha_{ent}}{R} \tag{1}$$

where α_{ent} is a dimensionless parameter currently set to 0.2. The parcel radius, R, is based on a turbulence length-scale in the parcel's source-layer given by $R = a_L K_M / \sigma_w$, where K_M is the momentum diffusivity in the boundary layer scheme and a_L a constant taken to be 0.45; $\sigma_w = (K_M/\tau)^{0.5}$ is a turbulent velocity scale where τ is a turbulent timescale, see Van Weverberg et al. (2016). Initial testing in the global model, however, found this simple formulation was insufficient to remove instability fast enough under all circumstances and so an additional scaling was introduced, increasing a_L based on an ad-hoc linear function of the previous time step's precipitation rate (up to a factor of 2 for a precipitation rate above approximately 35 mm per day). Qualitatively this can be viewed as allowing the updraft size to respond to the organisation of convection via precipitation leading to the formation of cold pools and subsequent initiation of larger-scale updraughts (Mapes and Neale (2011)). The parcel radius increases with height through entrainment by assuming the mass-flux is carried by a fixed number-flux of spherical thermals whose radii increase consistent with the increase in volume of each thermal.

The detrainment rate is modelled as removing the non-buoyant part of an assumed distribution of buoyancy within the bulk plume, informed by separate parcel ascent calculations for parcel mean and less dilute core properties. Importantly, this detrainment calculation is solved implicitly, in which the convective heating of the environment (as well as the other model increments through the timestep) is accounted for in the calculation of the parcels' buoyancy and therefore the proportion of the buoyancy distribution that is detrained.

The initiating parcel mean properties are calculated separately within each clear or cloudy sub-grid region, as with massflux initiation, and then averaged together weighted by their respective initiating massfluxes. The in-region properties are taken as just saturated and neutrally buoyant and then given a perturbation, ϕ', linked to the parametrized turbulent flux ($\phi' = \alpha_t \overline{w'\phi'}/\sigma_w$ with $\alpha_t = 1/3$ and ϕ being temperature, water vapour mixing ratio and the horizontal wind components). Because the parcel core is representing the most extreme tail of the distribution of sub-grid fluctuations, the core property perturbations are scaled up by a factor of 3.

As with the control, CoMorph uses a massflux representation of momentum transport by convection that also includes the effects of cloud pressure-gradients on the flow within the cloud (e.g., Kershaw and Gregory (1997)).

Importantly, CoMorph also includes a novel in-parcel bulk microphysics scheme for the generation of hydrometeors. These hydrometeors are then passed on the model-level where they leave the parcel (through detrainment and a fall-out flux) to the grid-scale microphysical variables. This can be achieved because, as~~As~~ in the control, the model's grid-scale (Wilson-Ballard) microphysics scheme prognoses the mass concentration of each hydrometeor species ~~and~~so convection can now provide~~s~~ an additional source term for these prognostics. Their fall to the surface, and any interactions on the way down, is modelled by the Wilson-Ballard scheme which therefore improves the consistency of treatment of precipitation between that generated through convective processes and that through larger, resolved scale ones. Note that diagnostically this means there is no longer any separation into convective or large-scale precipitation, just precipitation. In order for convection to modify rain mass and area fraction consistently a prognostic precipitation area fraction is introduced and passed to the large-scale microphysics. In addition to cloud liquid water, ice and rain, CoMorph itself includes graupel, which is not represented explicitly in the control model, being largely a feature of deep convection which is entirely parametrized there, but passing CoMorph's graupel to the large-scale's single ice variable led to far too excessive build-up of cloud ice in the tropics and so the large-scale microphysics' prognostic graupel was also included in the CoMorph-A package (following the configuration already used in the regional configurations of the UM, see Bush et al. (2020)). This initial implementation of a microphysics scheme in CoMorph is relatively simple, prescribing a representative number concentration for each hydrometeor species in order to calculate an effective particle size and thence fall speeds, accretion rates and other exchanges between hydrometeor classes. Crucially this allows the parcel (and detrained air) to become supersaturated with respect to ice, whereas the convection scheme in the control adjusts the parcel fully to ice-saturation when below the melting point temperature.

CoMorph is also written in terms of mixing ratios of water vapour and condensate (while the control convection scheme uses specific quantities). This has then allowed all the model's physics schemes to move across to using mixing ratios, consistent with the dynamical core, and so avoid conversions in moving between different parts of the model which allows global water conservation errors to be reduced to negligible levels.

In summary, the key aspects of the CoMorph convection scheme are:

- it is a single unified scheme for all convective regimes
- it is closely integrated with the rest of the model physics, giving greater physical consistency
- massflux is initiated through local moist instability leading to a much tighter coupling with the resolved dynamics of the model

- close attention has been paid to the numerical methods used, with substantial aspects solved implicitly, and this leads to a smooth temporal behaviour
- it includes a microphysical representation of cloud process in its updraughts and precipitation is passed directly to the prognostic grid-scale microphysical variables instead of being rained out diagnostically, thereby improving consistency of treatment of microphysical processes in the model

3.2 | Other model changes

3.2.1 | Cloud scheme

The impact of triggering CoMorph from either saturated or unsaturated air makes it sensitive to the diagnosis of the fraction of the grid box that is cloudy. In the process of developing CoMorph, several aspects of the PC2 cloud scheme were discovered to be excessively sensitive to small perturbations. Largely motivated, then, by a desire to reduce the timestep level variability of convection, the following changes were made to the PC2 cloud scheme:

- to ensure the cloud is consistent with the thermodynamic profiles at the point in the timestep where these are passed to CoMorph, the PC2 homogeneous forcing calculation from advection is moved from the end of the timestep to just after the advection calculation (which is called before convection) and new calls to the PC2 initiation and checking algorithms are added before the call to CoMorph
- the "BiModal" scheme of Weverberg et al. (2021) is used for initiation of cloud within PC2 (because of its more realistic treatment of subgrid variability), together with using that initiated cloud as a minimum cloudiness (cloud fraction and liquid water content) at every grid-point on every timestep (in the control the cloud has to dissipate completely before initiation is triggered which can lead to sudden large changes in cloud fraction)
- for consistency, the pressure change experienced by the environment as it undergoes convectively forced subsidence is used to drive the homogeneous forcing of cloud, following the same method as for resolved advection (Wilson et al. (2008a)), a process not treated explicitly in the control
- an implicit numerical method is introduced to calculate the PC2 term for the erosion of cloud, which depends on the cloud fraction (see Morcrette (2012)), such that the erosion rate applied is consistent with the cloud-fraction that will occur after the erosion increment has been added on
- the method of Morcrette (2020) is used to ensure that the PC2 cloud scheme produces reasonable magnitude cloud fraction increments in the limit of small condensate amounts

3.2.2 | Cloud microphysics

As discussed in section 3.1, the main changes to microphysics are to include graupel as a prognostic variable, which allows for the explicit representation of a second, more dense ice category, and to include a fractional area of precipitation so as to discriminate convectively generated rain that occupies a small fraction of the grid box from that generated by large-scale processes. Another, more minor, improvement is to relax the shallow atmosphere assumption in the calculation of flux divergences, and so be consistent with the rest of the model, which improves local conservation of water.

3.2.3 | Fountain Buster

In the absence of sufficient lateral subgrid mixing, the MetUM has been found susceptible to the formation of near-grid-scale flow structures that, combined with the lack of inherent conservation with semi-implicit semi-Lagrangian advection, leads to significant conservation errors. This problem can be illustrated by considering an idealised up-draught in a single grid-column with continuity requiring a convergent in-flow in lower levels. The interpolation of the Arakawa C staggered horizontal wind fields onto scalar points, however, strongly reduces resolved lateral convergence from surrounding points into grid-scale vertically ascending plumes. As a result, the vertical transport of, for example, water vapour away from the near surface is not compensated for by horizontal convergence of drier air into the plume from the sides, with the result that moisture can be transported vertically ad infinitum. Typically this is then manifested as extreme local precipitation accumulations. The use of a posteriori global conservation correction has been found to reduce these errors significantly (Bush et al. (2020)), but substantial local errors have been found to remain.

Here a post-hoc local correction is applied after the semi-Lagrangian scheme's interpolation to the departure point, in the form of the linear up-wind advection increments that arise from the convergent part of the flow that is removed when the horizontal wind components are interpolated to the scalar grid points for the departure point calculation. In more detail, first, at each lateral cell face a measure of the (assumed missing) convergent stagnation in-flow, S, is calculated. For example, for the west cell face of scalar point (i, j, k):

$$S_{\mathrm{west}} = \frac{u_{i-1,j,k} - s_d u^{\theta}}{u_{i-1,j,k}} \tag{2}$$

where u^{θ} is a linear estimate of u at the scalar point. To ensure only the convergent part of the flow is accounted for, we ensure $0 < S_{\mathrm{west}} < 1$, and to avoid making increments in reasonably well-resolved flows the tuning factor, s_d, is set to 2.

The fountain buster tendency for a scalar variable χ is then given by first-order upwind advection scaled by S, i.e.:

$$\begin{aligned} \frac{\Delta \chi_{i,j,k}}{\Delta t} &= S_{\mathrm{east}} u^{f}_{i,j,k} \frac{\chi_{i+1,j,k} - \chi_{i,j,k}}{\Delta x} - S_{\mathrm{west}} u^{f}_{i-1,j,k} \frac{\chi_{i,j,k} - \chi_{i-1,j,k}}{\Delta x} \\ &+ S_{\mathrm{south}} v^{f}_{i,j-1,k} \frac{\chi_{i,j,k} - \chi_{i,j-1,k}}{\Delta y} - S_{\mathrm{north}} v^{f}_{i,j,k} \frac{\chi_{i,j+1,k} - \chi_{i,j,k}}{\Delta y} \end{aligned} \tag{3}$$

where the superscript ^{f} denotes the wind interpolated (vertically) to the face centre of the scalar point. In (3) a regular cartesian grid has been used for simplicity but in the MetUM the appropriate metric variables are used. The fountain buster is applied to all advected scalar variables, so all moisture variables, tracers and the thermodynamic variable (dry virtual potential temperature).

3.2.4 | Turbulent mixing

A deliberate choice in the Lock et al. (2000) boundary layer scheme was to interface with the convection scheme at the lifting condensation level (LCL, diagnosed from the top of the surface layer), meaning that the boundary layer scheme would be entirely responsible for surface-driven mixing at least up to the LCL, from where the convection scheme would then be initiated and take over the transport into the free troposphere. With CoMorph, initiation can now occur at any level and so we take the opportunity to relax the requirement that the boundary layer scheme mix up to this definition of the LCL. We still use the Lock et al. (2000) undilute moist adiabatic parcel ascent method to diagnose the potential for cumulus convection but, in those regimes, now diagnose the top of the surface-driven turbulence diffusion profile as the point where the integral of diagnosed negative buoyancy flux is a fraction (0.05, see Walters et al. (2019)) of the vertical integral of the positive flux. Because we assume any transport within clouds will be carried by CoMorph, we use the unsaturated buoyancy flux in this calculation.

A second alteration to the boundary layer scheme is in the calculation of the buoyancy gradient used in the Richardson number (Ri). This is revised to reduce the mixing from the Ri-dependent part of the scheme across statically stable inversions, in particular where these cap a cloudy boundary layer. With the UM's Charney-Philips vertical grid staggering, Ri is required on the same grid-level as scalars (referred to as θ-levels), where the vertical gradient of horizontal momentum naturally falls. In the control, the gradients of liquid-ice static energy temperature and total water content are interpolated to θ-levels and that θ-level's cloud fraction used to obtain the buoyancy gradient. It is found that at cloudy θ-levels below a strong inversion this interpolation of the gradients, combined with a saturated buoyancy calculation, can lead to apparent instability. In the CoMorph-A package we calculate the buoyancy gradient locally (on ρ-levels) and interpolate that to the θ-levels. To calculate the saturated contribution to the buoyancy gradient on ρ-levels, an estimate of the vertical fraction of the grid containing saturated air is made from interpolating the supersaturation in the adjacent θ-levels. In this way the contribution from the ρ-level with strong gradients is typically largely unsaturated, leading to strong stability, which then remains stable when averaged with the saturated ρ-level with weak gradients below.

As with the Fountain Buster, the more active dynamics in the tropics arising from more organised convection with CoMorph also motivates enabling the Leonard terms (Hanley et al. (2019)), which include extra subgrid vertical fluxes that account for the tilting of horizontal flux into the vertical by horizontal gradients in vertical velocity. Including these terms helps to weaken a few occurrences of excessively strong resolved updraughts and precipitation in organised convective structures.

3.3 | Tuning of the top-of-atmosphere radiation

As with any major model developments, the initial simulations showed significantly worse biases than the control, both locally and globally in the top-of-atmosphere radiation. To reduce excessively weak outgoing longwave radiation

(OLR) in the tropics, we increased the fall speeds for cloud ice by 20% (which increases the global mean OLR by around 1.5 Wm^{-1} and reduces the spatial root-mean-square error (rmse) against satellite climatology (see section 4) by 0.3 Wm^{-1}) and also removed a parametrization in PC2 that increased the ice cloud fraction through vertical wind shear that was not especially well justified physically (which increased the global mean OLR, by 0.5 Wm^{-1}, and reduced the rmse by 0.3 Wm^{-1}). In the shortwave (SW), the cloud forcing was initially too strong across most of the tropics. Several options are available that can reduce the reflectivity of clouds and we have made two revisions. The first was to the parameters in the Liu et al. (2008) spectral dispersion of the cloud droplet size distribution. As described in Mulcahy et al. (2018), the cloud droplet spectral dispersion as implemented in the control is given by

$$\beta = a\left(\frac{L}{N_d}\right)^b \tag{4}$$

where L is the cloud liquid water content and N_d the cloud droplet number concentration. In the control $a = 0.07$ and $b = -0.14$ while in the CoMorph-A package we use $a = 0.093$ and $b = -0.13$. These changes, that are small compared to the spread in the Liu et al. (2008) data, resulted in a reduction in global mean reflected SW of around 1.5 Wm^{-1}, whilst having almost no impact on OLR. Regionally the SW impact was strongest broadly across the marine sub-tropics and gave a reduction in spatial rmse of around 1 Wm^{-1}. Our second tuning, to further reduce the reflectivity of clouds, was to increase a parameter in the fractional standard deviation of liquid clouds (equal to the standard deviation of cloud water content in a grid box divided by its mean value, see Hill et al. (2015)) from 1.6 to 1.65, which reduced the global mean reflected SW by around 0.7 Wm^{-1} and the spatial rmse by 0.25 Wm^{-1}. Note, though, that the impacts of these last two changes would certainly be different if implemented in the reverse order.

It is important to remember that this tuning is a critical step in any new physics package and was, of course, also done for the control configuration. Hence the impacts discussed in section 4 should be viewed as resulting from the CoMorph-A package as a whole.

3.4 | Cost

There is a marginal increase in the CPU time with CoMorph-A of roughly 5% over the control of which a substantial part will be the new prognostic graupel - tests with just the convection scheme reverted to that in the control show a similar increase indicating the CoMorph convection scheme itself is cost neutral.

4 | RESULTS IN AMIP

We evaluate the climatology of the CoMorph-A package using AMIP simulations at N96 resolution (around 135 km grid spacing in mid-latitudes). Given the main change is to the convection parametrization, we start by looking in Fig. 1 at the impact on the annual mean precipitation. The most systematic change is to have increased rain over tropical land, including the maritime continent, most of which is beneficial compared to the Global Precipitation Climatology

Project (GPCP, Adler et al. (2003)). Particularly relevant for the Maritime Continent, a significant issue noted by operational meteorologists with the control simulation in the tropics is precipitation in convective weather systems abruptly stopping at the coastline as they move from sea to land. This issue is much improved in CoMorph-A. Especially over the Pacific Ocean there is a sharpening of the ITCZ, giving enhanced rainfall on the equator with reductions to the north and south, with mixed impact.

More detailed analysis shows the characteristics of the model's tropical precipitation at local time and space scales are altered beyond recognition. Fig. 2 quantifies the probability of grid point precipitation rates at each timestep given the rate at the previous timestep. In the control model there is a strong signal along the axes, indicating a high probability of no precipitation on one timestep if there was precipitation on the previous, and vice versa – this illustrates the long-standing, Klingaman et al. (2017), time-step level intermittency in the control. With CoMorph-A this timestep intermittency is completely removed and shows a far more plausible temporal coherence with high probabilities around the one-to-one line. ~~Fig. 2 shows that the local characteristics of tropical precipitation are altered beyond recognition, with the long-standing Klingaman et al. (2017) time-step level intermittency in the control completely removed in CoMorph-A, which shows a far more plausible correlation.~~ This continuity between time steps is a direct result of the use of improved numerical methods, as discussed in section 3, and the implicit solution for detrainment in CoMorph, in particular, as this will tend to maintain similar convective inhibition into the next time step. Interestingly, after averaging over 3 hours and 2x2 grid points for comparison with the GPM observations (Global Precipitation Measurement (GPM) Multi-satellitE Retrievals (IMERG) precipitation data V06B, Tan et al. (2019)), the models' precipitation characteristics are far more similar. This convergence is similar to that seen for a range of MetUM configurations at various resolutions in Martin et al. (2017) and similar to the results for a number of CMIP5 models (except for those with particularly coarse resolution) in Klingaman et al. (2017). There is, nevertheless, a suggestion of more temporally coherent heavy rain with CoMorph-A, closer to GPM, albeit still insufficient. It is also interesting to reflect that many of the geographical biases in tropical precipitation seen in Fig. 1 are remarkably similar, despite entirely replacing the convection scheme, although many of these simply reflect the regions with the heaviest rainfall.

The strength of propagating tropical waves is strongly improved, see Fig. 3, both for Kelvin waves (as marked on the figure) and the Madden-Julian Oscillation (MJO, the region of strong observed eastward-propagating 30–60 day variability at wave numbers 1 to 3). We believe this tighter coupling between CoMorph and the resolved dynamics arises because the initiation of massflux can respond to locally generated moist instability, but more detailed investigation will be the subject of future work.

Fig 4 shows a large increase in the integrated tropical water vapour that all but removes a dry bias in the control, largely occurring in the upper troposphere. Around a half of that moistening comes from the Fountain Buster scheme, while the rest is likely due to passing the precipitation into the "large-scale" microphysics that then represents its evaporation as it falls to the surface more realistically (although to confirm this would require adding some form of direct precipitation to the surface within CoMorph, which is beyond the scope of this work). This moister troposphere may also contribute to the improvement in the strength of tropical waves, see Fig. 3 (Zhu et al. (2023a)).

There are also substantial changes to the clouds in the model, as seen in the top-of-atmosphere cloud radiative effect (CRE, which is the clear-sky minus the total radiative flux). The longwave CRE, Fig. 5, is much stronger across the tropics and especially over tropical land, which all but eliminates a serious underestimate in the control. This is due to a large increase in the tropical ice cloud amount (both mass and cloud fraction) as can also be seen in the comparison with CALIPSO observations over central Africa in Fig. 6, likely arising from the handling of precipitation sedimentation by the grid-scale microphysics. However, like the control, there is less cloud than observed by CALIPSO between 5km and 8km altitude suggesting that the congestus phase remains poorly simulated. The increase in optically thick cirrus means shortwave CRE (Fig. 7) is also enhanced somewhat over tropical land, but the biggest impacts here are in the subtropics and especially over the eastern Pacific and Atlantic. Climatalogically, these are areas dominated by stratocumulus clouds. The geographical pattern of the change from including the CoMorph-A package matches remarkably well with the error in the control, although the end result is for the clouds to be somewhat too reflective over most of the tropical oceans. Part of the increase in stratocumulus arises from the implementation of BiModal initiation in the PC2 cloud scheme and the revised calculation of Ri, but around half comes from CoMorph itself, especially further west from the coastline where shallow cumulus clouds form under the lifting stratocumulus. Detailed single column model analysis of this transition region (not shown) indicates that the combination of the smoother temporal evolution of CoMorph (as in Fig 2) and more sensitive (implicit) detrainment allow a smoother evolution of the stratiform cloud layer as it rises away from the coast. Consistent with the improved top-of-atmosphere radiative fluxes, we also find the net surface energy fluxes (that are important for coupled ocean modelling) are significantly improved, and across the tropics and subtropics especially, compared to the observed estimate from Liu et al. (2015) (not shown).

A form of convective "memory" was implemented in the control model (in GA8GL9 relative to GA7GL7, as described in section 2) to delay the development of deep convection and help address the poor representation of the diurnal cycle of precipitation over land. However, consistent with other studies (Willett and Whitall (2017); Tao and et al (2024)), we find GA8GL9 still has issues in simulating the correct timing of the diurnal cycle over many areas of the globe (see Fig. 8). CoMorph-A does not have such a memory function and~~CoMorph-A does not contain a form of "memory", unlike the control. Consequently, it~~ has a tendency to have the diurnal peak in rainfall intensity over tropical land around local noon or early afternoon, compared to the observed late evening peak (Fig. 8). Over some regions (e.g. Africa) this is earlier and hence detrimental compared with the control, whilst over others (e.g. S. E. Asia, as also seen in Zhu et al. (2023b)) CoMorph-A is an improvement on the control, although still considerably earlier than observed. Diurnal cycle experiments using the idealised MetUM (Lavender et al. (2024)) also show too early initiation and development to deep convection using CoMorph-A compared to high resolution simulations, although improved relative to the control.

5 | RESULTS IN NWP

The NWP trials (cycling forecasts and data assimilation) are performed at somewhat higher, N320 (~ 40 km in mid-latitudes), resolution than the climate simulations presented in section 4. A wide variety of metrics are monitored and these are summarised in the "scorecards" shown in Fig. 9. These illustrate the change in root-mean-square error (rmse) against each trial's own analysis (scorecards are also produced against observations and independent global analyses from ECMWF but those look very similar so are not shown). The majority of metrics show reductions in rmse with

CoMorph-A, with somewhat better overall performance in the boreal summer than winter (overall reductions of 1.9% and 0.5% respectively). Some degradation is seen in a number of fields in the first two days that may arise from not updating the error covariance statistics in the trials. One field that shows degradation throughout the forecasts in both summer and winter, though, is the tropical temperature at 850 hPa. Fig. 10 shows the geographical distribution of the change in rmse at day 6, which has large positive values across most of the tropical oceans but especially so, for these austral summer trials, in the sub-tropical south-eastern Pacific and Atlantic close to the edges of where CoMorph-A gives more stratocumulus cloud layers (the NWP trials show a similar increase to that shown to be beneficial in the AMIP simulations in Fig. 7). Fig. 10 also shows that the standard deviation of temperature at 850 hPa in the analyses is increased in CoMorph-A, and the day 6 forecasts in CoMorph-A have similarly more variable temperatures at this level (not shown). The more persistent stratocumulus clouds with CoMorph-A will result in a sharper temperature inversion at the top of the boundary layer. Furthermore, on the western edge (and further downwind) of the stratocumulus, there is more variability of the cloud cover as it transitions to shallow cumulus. These transitions result in variations in the height of the inversion which will be manifested as increased temperature variability and rmse at this level, even if the average inversion height or boundary layer temperature were accurately forecast (the 1000 hPa temperature rmse is actually improved or neutral over tropical oceans, not shown).

A long standing systematic error is a slow bias in the winter extra-tropical jet. Fig. 11 shows an increase in the wind speed from CoMorph-A, reducing this error. It is often the case that increasing the wind speed will also increase the rmse due to a “double penalty” if a wind feature is geographically displaced. It is notable, therefore, that CoMorph-A reduces the slow bias with an overall neutral impact on rmse for upper level winds (Fig. 11 & Fig. 9).

Further analysis of the trials has included tracking the location of extra-tropical cyclones through the maximum in 850 hPa vorticity (Hodges (1995)). Whilst the error bars overlap and hence cannot be regarded as significantly different, the errors in these tracks are reduced in CoMorph-A and experience suggests the fact the signal is consistent in the two seasons is notable (Fig. 12).

Finally, between 25 June to 31 October 2021, atmosphere-only forecasts with the CoMorph-A package were run daily at the operational resolution of N1280 from Met Office operational analyses at 0 UTC. Verification of tropical cyclones from these forecasts in Fig. 13 shows CoMorph-A gave substantial deepening and improvement to wind speeds. Whilst the central pressure in these simulations is now lower than observed, they are atmosphere-only and we would expect slower-moving storms to be weaker when coupled to an ocean model in operational systems.

6 | CONCLUSIONS

The results from a range of global simulations have been presented for a large package of revised parametrization schemes, centred around the entirely new CoMorph massflux convection scheme. The key components of CoMorph are that it has a physically-based flexible formulation that allows it to represent all convective regimes and is tightly coupled to the rest of the model, both the other parametrization schemes and the dynamics. The main impacts of this overall CoMorph-A package in standard global test simulations are found to be:

- removal of the timestep level intermittency of convection that has been in all configurations of the MetUM since its inception
- improved tropospheric humidity over tropical land
- improved tropical variability, including Kelvin waves and MJO
- surface fluxes improved in many regions, important when coupling to an ocean model
- increased high cloud over tropical land where it has always been lacking and hence marks a significant improvement
- increased low cloud over tropical oceans which is generally better but optically too bright everywhere (although tuned for the global mean net top-of-atmosphere radiative flux, in order to balance weak clear sky out-going longwave radiation)
- improved NWP performance, including reduced tropical and extra-tropical cyclone errors
- some degradation of the diurnal cycle of tropical precipitation

Given the extent of new developments within the CoMorph-A package, this represents impressive performance for a first implementation of a new convection scheme. Future work will focus on improving the diurnal cycle, through for example inclusion of a second updraught to represent, separately, convection forced from cold pools, and on CoMorph's applicability to higher resolutions, where the larger scales of convection begin to be resolved.

Acknowledgements

The contributions of A. P. Lock and M. Willett were supported by the Met Office Hadley Centre Climate Programme funded by DSIT. The contributions of M. Whitall, P. R. Field and G. Martin were supported by the Met Office Weather and Climate Science for Service Partnership (WCSSP) India, a collaborative initiative between the Met Office and the Indian Ministry of Earth Sciences (MoES). The contributions of M. Whitall, A. J. Stirling, K. D. Williams and M .Willett were supported by WCSSP Southeast Asia. The WCSSP programme is supported by the U.K. Government's Newton Fund. S. L. Lavender is funded through the Northern Australia Climate Program (NACP), funded by Meat and Livestock Australia, the Queensland Government through the Drought and Climate Adaptation Program, and the University of Southern Queensland. K. Matsubayashi was a visiting scientist working at the Met Office on secondment from the Japan Meteorological Agency under agreement number L4183. We also thank Duncan Ackerley for his help with the mid-latitude cyclone analysis. This work was carried out as part of the joint Met Office-NERC ParaCon programme (https://www.metoffice.gov.uk/research/approach/collaboration/paracon) and we are grateful to the ParaCon community for many stimulating discussions.

Data availability statement

The data that support the findings of this study are available from the corresponding author and Met Office co-authors upon reasonable request.

References

Adler, R. F., Huffman, G. J., Chang, A., Ferraro, R., Xie, P.-P., Janowiak, J., Rudolf, B., Schneider, U., Curtis, S., Bolvin, D., Gruber, A., Susskind, J., Arkin, P. and Nelkin, E. (2003) The version-2 global precipitation climatology project (gpcp) monthly precipitation analysis (1979–present). *J.Hydrometeor.*, **4**, 1147–1167.

Ahn, M.-S., Kim, D., Kang, D., Lee, J., Sperber, K. R., Gleckler, P. J. and et al (2020) Mjo propagation across the maritime continent: Are cmip6 models better than cmip5 models? *Geophysical Research Letters*, **47**.

Arakawa, A. and Schubert, W. H. (1974) Interaction of a cumulus cloud ensemble with the large-scale environment, part i. *J. Atmos. Sci.*, **31**, 674–701.

Bain, C. L., Williams, K. D., Milton, S. F. and Heming, J. T. (2014) Objective tracking of african easterly waves in met office models. *Q.J.R. Meteorol. Soc.*, **140**, 47–57.

Bush, M., Allen, T., Bain, C., Boutle, I., Edwards, J., Finnenkoetter, A., Franklin, C., Hanley, K., Lean, H., Lock, A., Manners, J., Mittermaier, M., Morcrette, C., North, R., Petch, J., Short, C., Vosper, S., Walters, D., Webster, S., Weeks, M., Wilkinson, J., Wood, N., and Zerroukat, M. (2020) The first met office unified model–jules regional atmosphere and land configuration, ral1. *Geosci. Model Dev.*, **13**, 1999–2029.

Christopoulos, C. and Schneider, T. (2021) Assessing biases and climate implications of the diurnal precipitation cycle in climate models. *Geophysical Research Letters*, **48**.

Daleu, C. L., Plant, R. S., AJ, S. and Whitall, M. (2023) Evaluating the comorph parameterization using idealised simulations of the two-way coupling between convection and large-scale dynamics. *Quart. J. Royal Meteorol. Soc.*, **149**, 3087–13109.

Derbyshire, S., Maidens, A., Milton, S. F., Stratton, R. A. and Willett, M. R. (2011) Adaptive detrainment in a convective parametrization. *Q.J.R. Meteorol. Soc.*, **137**, 1856–1871.

Dias, J., Gehne, M., Kiladis, G. and Magnusson, L. (2023) The role of convectively coupled equatorial waves in sub-seasonal predictions. *GRL*, **50**.

Edwards, J. and Slingo, A. (1996) Studies with a flexible new radiation code. i: Choosing a configuration for a large-scale model. *Q.J.R. Meteorol. Soc.*, **122**, 689– 719.

Fletcher, J. and Bretherton, C. (2010) Evaluating boundary layer–based mass flux closures using cloud-resolving model simulations of deep convection. *J. Atmos. Sci.*, **67**, 2212–2225.

Furtado, K. and Field, P. (2017) The role of ice-microphysics parametrizations in determining the prevalence of supercooled liquid water in high-resolution simulations of a southern ocean midlatitude cyclone. *Journal of the Atmospheric Sciences*, **74**, 2001–2021.

Gregory, D. and Rowntree, P. R. (1990) A mass flux convection scheme with representation of cloud ensemble characteristics and stability-dependent closure. *Mon. Wea. Rev.*, **118**, 1483–1506.

Hanley, K., Whitall, M., Stirling, A. and Clark, P. (2019) Modifications to the representation of subgrid mixing in kilometre-scale versions of the unified model. *Q. J. Roy. Meteorol. Soc.*, **145**, 3361–3375.

Hill, P. G., Morcrette, C. J. and Boutle, I. A. (2015) A regime-dependent parametrization of subgrid-scale cloud water content variability. *Q. J. Roy. Meteorol. Soc.*, **141**, 1975–1986.

Hodges, K. I. (1995) Feature tracking on the unit sphere. *Mon. Wea. Rev.*, **123**, 3458–3465.

Holloway, C., Petch, J., Beare, R., Bechtold, P., Craig, G., S.H., D., Donner, L., Field, P., Gray, S., Marsham, J., Parker, D., Plant, R., Roberts, N., Schultz, D., Stirling, A. and Woolnough, S. (2014) Understanding and representing atmospheric convection across scales: recommendations from the meeting held at dartington hall, devon, uk, 28–30 january 2013. *Atmospheric Science Letters*, **14**, 348–353.

Huffman, G. J., Adler, R. F., Bolvin, D. T., Gu, G., Nelkin, E. J., Bowman, K., Stocker, E. and Wolff, D. (2007) The trmm multi-satellite precipitation analysis (tmpa): quasi-global, multiyear, combined-sensor precipitation estimates at fine scales. *J. Hydrometeorol.*, **8**, 38–55.

Janiga, M. A. C. J. S., Ridout, J. A., Flatau, M., Barton, N. P., Metzger, E. J. and Reynolds, C. A. (2018) Subseasonal forecasts of convectively coupled equatorial waves and the mjo: Activity and predictive skill. *Mon. Wea. Rev.*, **146**, 2337–2360.

Kershaw, R. and Cregory, D. (1997) Parametrization of momentum transports by convection. i: Theory and cloud modelling results. *Q. J. R. Meteorol. Soc.*, **123**, 1133–1151.

Klingaman, N. P., Martin, G. M. and Moise, A. (2017) Asop (v1.0): a set of methods for analyzing scales of precipitation in general circulation models. *Geosci. Model Dev.*, **10**, 57–83.

Klingaman, N. P. and Woolhough, S. J. (2013) Using a case-study approach to improve the madden–julian oscillation in the hadley centre model. *Quart. J. Royal Meteorol. Soc.*, **140**, 2491–2505.

Lavender, S. L., Stirling, A. J., Whitall, M., Stratton, R., Daleu, C. L., Plant, R. S. and Lock, A. (2024) The use of idealised experiments in testing a new convective parameterization: Performance of comorph-A. *Accepted for Quart. J. Royal Meteorol. Soc.*

Liu, C., Allan, R., Berrisford, P., Mayer, M., Hyder, P., Loeb, N., Smith, D., Vidale, P.-L. and Edwards, J. (2015) Combining satellite observations and reanalysis energy transports to estimate global net surface energy fluxes 1985–2012. *JGR Atmospheres*, **120**.

Liu, Y., Daum, P. H., Guo, H. and Peng, Y. (2008) Dispersion bias, dispersion effect, and the aerosol–cloud conundrum. *Environ. Res. Lett.*, **3**.

Lock, A., Brown, A., Bush, M., Martin, G. and Smith, R. (2000) A new boundary layer mixing scheme. part i: Scheme description and single-column model tests. *Monthly Weather Review*, **128(9)**, 3187–3199.

Loeb, N., Wielicki, B. A., Wong, T. and Parker, P. A. (2009) Impact of data gaps on satellite broadband radiation records. *J. Geophys. Res. Atmos.*, **114**.

Manners, J., Edwards, J. M., Hill, P. and Thelen, J.-C. (2015) Socrates (suite of community radiative transfer codes based on edwards and slingo) technical guide. *Met Office, UK*.

Mapes, B. (2000) Convective inhibition, subgrid-scale triggering energy, and stratiform instability in a toy tropical wave model. *J. Atmos. Sci*, **57**.

Mapes, B. and Neale, R. (2011) Parameterizing convective organization to escape the entrainment dilemma. *Journal of Advances in Modeling Earth Systems*, **3**.

Martin, G. M., Klingaman, N. P. and Moise, A. (2017) Connecting spatial and temporal scales of tropical precipitation in observations and the metum-ga6. *Geosci. Model Dev.*, **10**, 105–126.

Morcrette, C. (2012) Improvements to a prognostic cloud scheme through changes to its cloud erosion parametrization. *Atmospheric Science Letters*, **13**, 95–102.

— (2020) Modification of the thermodynamic variability closure in the met office unified model prognostic cloud scheme. *Atmospheric Science Letters*, **22**.

Mulcahy, J. P., Jones, C., Sellar, A., Johnson, B., Boutle, I. A., Jones, A., Andrews, T., Rumbold, S. T., Mollard, J., Bellouin, N., Johnson, C. E., Williams, K. D., Grosvenor, D. P. and T., M. D. (2018) Improved aerosol processes and effective radiative forcing in hadgem3 and ukesm1. *Journal of Advances in Modeling Earth Systems*, **10**.

Sherwood, S., Bony, S. and Dufresne, J. (2014) Spread in model climate sensitivity traced to atmospheric convective mixing. *Nature*, **505**, 37–42.

Tan, J., Huffman, G. J., Bolvin, D. T. and J., N. E. (2019) Diurnal cycle of imerg v06 precipitation. *Geophys. Res. Lett.*, **46**, 13584–13592.

Tao, C. and et al (2024) Diurnal cycle of precipitation over the tropics and central united states: intercomparison of general circulation models. *Quart. J. Royal Meteorol. Soc.*, 1–26.

Tomassini, L. (2018) Mesoscale circulations and organized convection in african easterly waves. *J. Atmos. Sci.*, **75**, 4357–4381.

Uppala, S. M., KAllberg, P. W., J, S. A. and et al (2005) The era-40 re-analysis. *Q. J. Roy. Meteorol. Soc.*, **131**, 2961–3012.

Van Weverberg, K., Boutle, I., Morcrette, C. and Newsom, R. (2016) Towards retrieving critical relative humidity from ground-based remote-sensing observations. *Quart. J. Royal Meteorol. Soc.*, **142**, 2867–2881.

Vitart, F., Woolnough, S., Balmaseda, M. A. and Tompkins, A. M. (2007) Monthly forecast of the madden–julian oscillation using a coupled gcm. *Mon. Weather Rev.*, **135**, 2700—-2715.

Walters, D., Baran, A., Boutle, I., Brooks, M., Earnshaw, P., Edwards, J., Furtado, K., Hill, P., Lock, A., Manners, J., Morcrette, C., Mulcahy, J., Sanchez, C., Smith, C., Stratton, R., Tennant, W., Tomassini, L., van Weverberg, K., Vosper, S., Willett, M., Browse, J., Bushell, A., Carslaw, K., Dalvi, M., Essery, R., Gedney, N., Hardiman, S., Johnson, B., Johnson, C., Jones, A., Jones, C., Mann, G., Milton, S., Rumbold, H., Sellar, A., Ujiie, M., Whitall, M., Williams, K. and Zerroukat, M. (2019) The met office unified model global atmosphere 7.0/7.1 and jules global land 7.0 configurations. *Geosci. Model Dev.*, **12**, 1909–1963.

Weverberg, K. V., Morcrette, C. J., Boutle, I., Furtado, K. and Field, P. R. (2021) A bimodal diagnostic cloud fraction parameterization. part i: Motivating analysis and scheme description. *Mon. Weather Rev.*, **149**, 841–857.

Whitall, M., Stirling, A., Lavender, S., Stratton, R. and Matsubayashi, K. (2022) The comorph convection scheme. um documentation paper 043. *Technical report no. 617, Met Office*.

Willett, M. and Whitall, M. (2017) A simple prognostic based convective entrainment rate for the unified model: Description and tests. *Met Office*.

Williams, K. D., van Niekerk, A., Best, M. J., Lock, A. P., Brooke, J. K., Carvalho, M. J., Derbyshire, S. H., Dunstan, T. D., Rumbold, H. S., Sandu, I. and Sexton, D. M. H. (2020) Addressing the causes of large-scale circulation error in the met office unified model. *Q. J. Roy. Meteorol. Soc.*, **146**, 2597–2613.

Wilson, D. R. and Ballard, S. P. (1999) A microphysically based precipitation scheme for the uk meteorological office unified model. *Q. J. Roy. Meteorol. Soc.*, **125**, 1607–1636.

Wilson, D. R., Bushell, A. C., Kerr-Munslow, A. M., Price, J. D. and Morcrette, C. J. (2008a) Pc2: A prognostic cloud fraction and condensation scheme. i: Scheme description. *Q. J. Roy. Meteorol. Soc.*, **134**, 2093–2107.

Wilson, D. R., Bushell, A. C., Kerr-Munslow, A. M., Price, J. D., Morcrette, C. J. and Bodas-Salcedo, A. (2008b) Pc2: A prognostic cloud fraction and condensation scheme. i: Climate model simulations. *Q. J. Roy. Meteorol. Soc.*, **134**, 2109–2125.

Winker, D. M., Pelon, J. and McCormick, M. P. (2002) The calipso mission: Spaceborne lidar for observation of aerosols and clouds. *Proc. SPIE*, **4893**, 1–11.

Wood, N., Staniforth, A., White, A., Allen, T., Diamantakis, M., Gross, M., Melvin, T., Smith, C., Vosper, S., Zerroukat, M. and Thuburn, J. (1999) An inherently mass-conserving semi-implicit semi-lagrangian discretization of the deep-atmosphere global non-hydrostatic equations. *Q. J. Roy. Meteorol. Soc.*, **140**, 1505–1520.

Xie, S.and Ma, H., Boyle, J., Klein, S. and Zhang, Y. (2012) On the correspondence between short- and long-time-scale systematic errors in cam4/cam5 for the year of tropical convection. *J. Climate*, **25**, 7937–7955.

Yang, G.-Y. and Slingo, J. (2001) The diurnal cycle in the tropics. *Mon. Weather Rev.*, **129**, 784–801.

Zhu, H., H., H. and C., J. (2023a) Convection in a parameterized and super-parameterized model and its role in the representation of the mjo. *J. Atmos. Sci.*, **66**, 2796–2811.

Zhu, H., Hudson, D., Li, C., Shi, L., Young, G., Stirling, A., Whitall, M., Lock, A., Lavender, S. and Stratton, R. (2023b) Impacts of the new um convection scheme, comorph-a, over the indo-pacific and australian regions. *Submitted to Journal of Southern Hemisphere Earth Systems Science*.

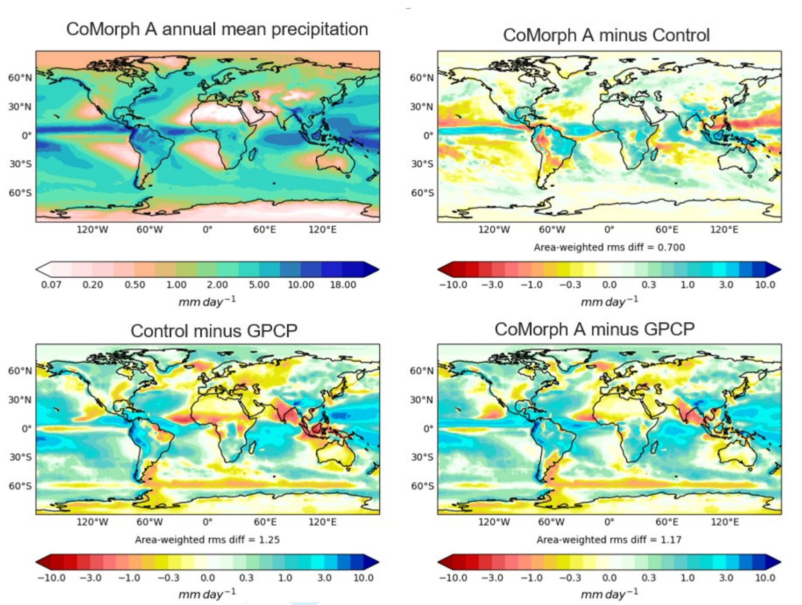

FIGURE 1 Annual mean precipitation biases compared to GPCP observations from N96 AMIP simulations

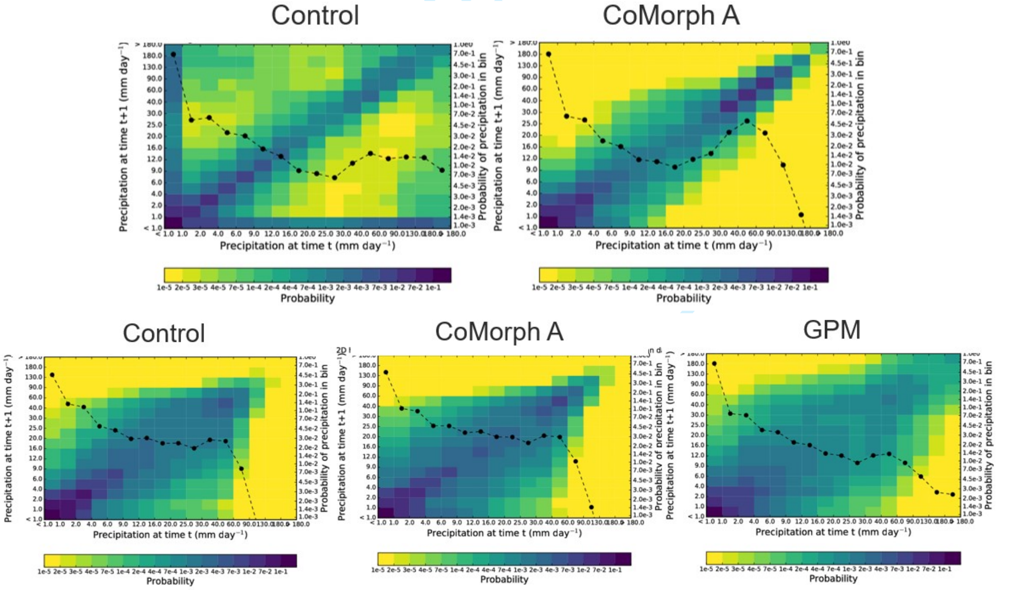

FIGURE 2 Histograms of the probability of bins of precipitation, measured at the time step and grid point level (top row) and over 3 hourly and 2x2 grid box averages (bottom row), aggregated over all grid points in the equatorial Indian Ocean from N96 AMIP simulations. The dashed lines show the one-dimensional histogram of the binned precipitation, using the right-hand vertical axis.

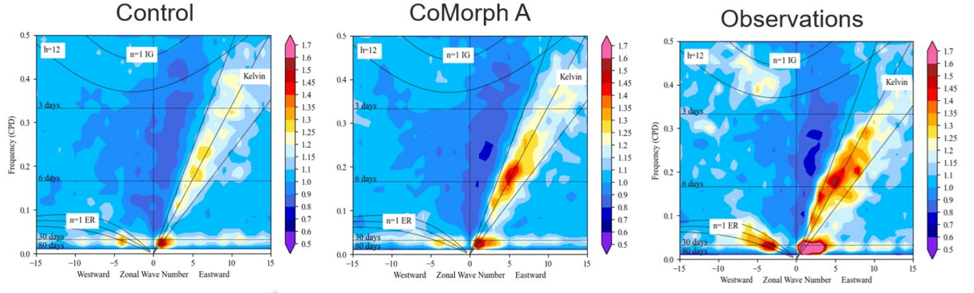

FIGURE 3 Wavenumber – frequency spectra of symmetric component of precipitation divided by the background power from N96 AMIP simulation. The observations are from TRMM 3B42 (Huffman et al. (2007))

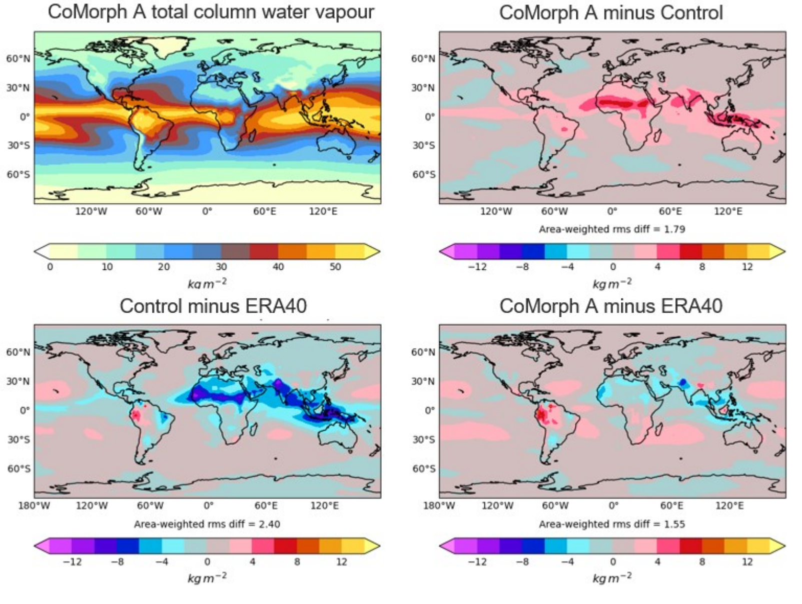

FIGURE 4 Annual mean total column water vapour from N96 AMIP simulations, and compared to ERA40 (Uppala et al. (2005)) in the bottom row.

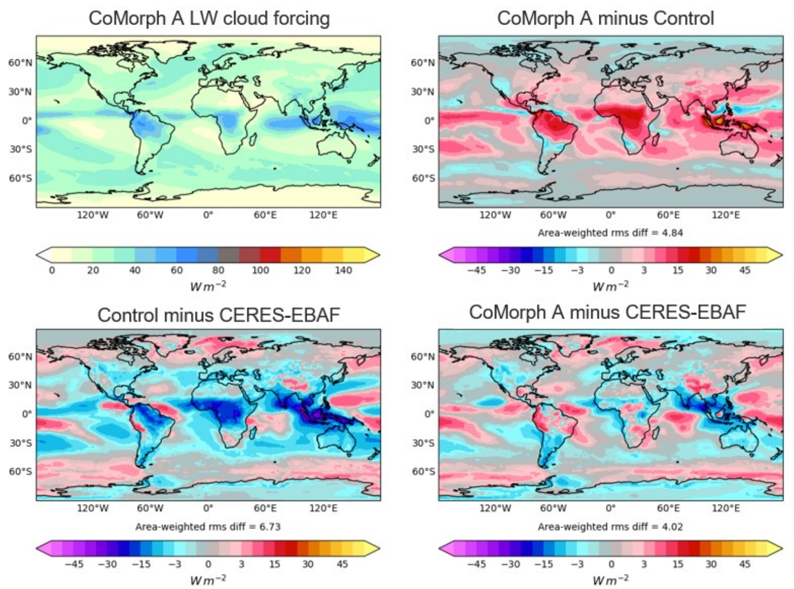

FIGURE 5 Longwave cloud radiative effect compared to Clouds and the Earth's Radiant Energy System (CERES) Energy Balanced and Filled (EBAF) dataset (Loeb et al. (2009)) from N96 AMIP simulations

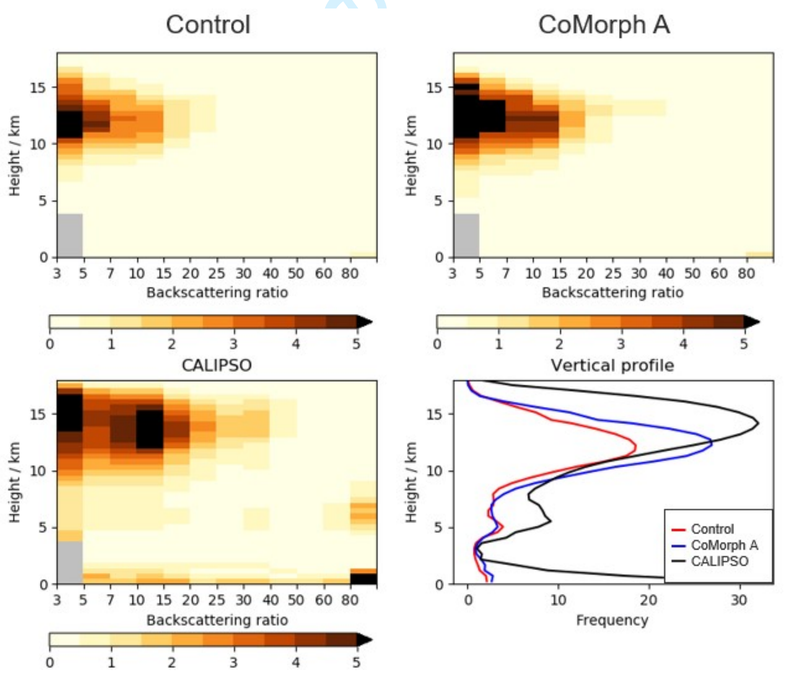

FIGURE 6 Histograms of height vs 532nm lidar backscatter ratio over central Africa (15^{o}E-30^{o}E, 20^{o}S-10^{o}N), showing climatologies of CALIPSO observations (Winker et al. (2002)) and simulated climatologies of CALIPSO data from 20-year N96 atmosphere/land-only climate simulations from the control and CoMorph-A

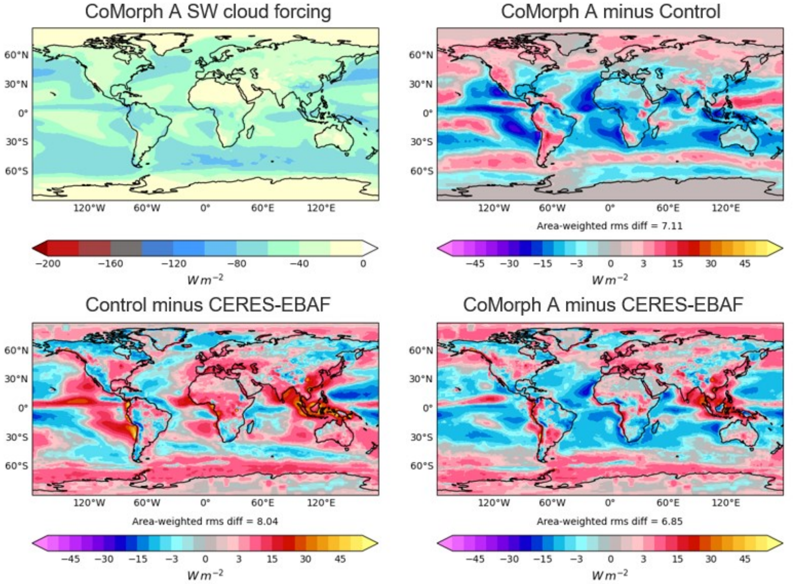

FIGURE 7 Shortwave cloud radiative effect compared to CERES-EBAF from N96 AMIP simulations

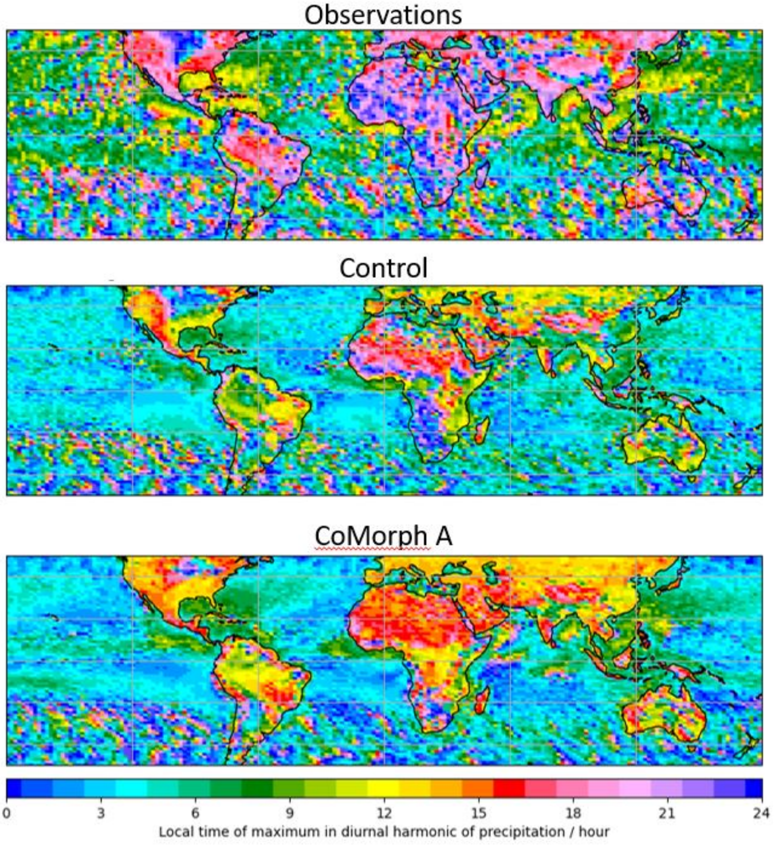

FIGURE 8 Local time of maximum in the diurnal harmonic of precipitation during JJA compared to TRMM 3B42 observations

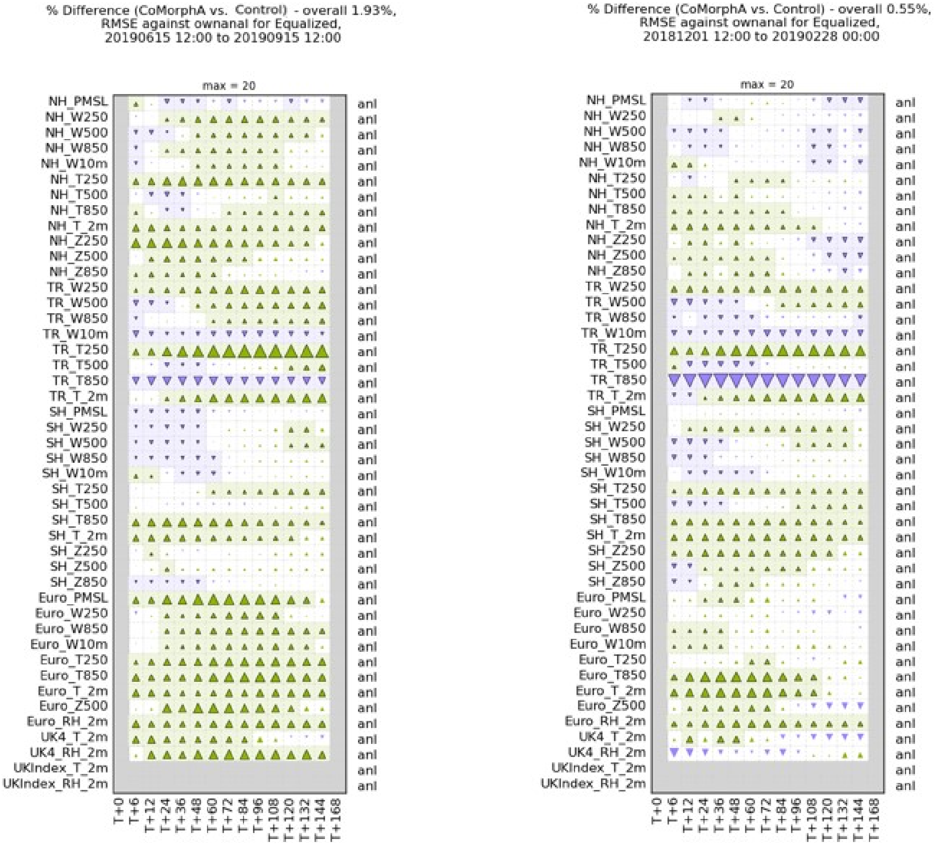

FIGURE 9 Scorecards against own analysis from the summer (left) and winter (right) NWP trials. Green upward triangles indicate reductions in root-mean-square error (rmse) and purple downward triangles increases, with the size of each scaled by the magnitude of change. Parameters are evaluated in the Northern Hemisphere (NH, north of 18.75° N), the tropics (TR, within 18.75° of the equator), the Southern Hemisphere (SH, south of 18.75° S), Europe (Euro) and UK (UK4 and UKIndex). The parameters are pressure at mean sea level (PMSL), vector wind (W), temperature (T) and geopotential height (Z) at various pressure levels given in hectopascals (such that NH_T250, for example, measures the change in rmse temperatures at 250 hPa in the northern hemisphere region). The columns represent forecast ranges from 6 h (T+6) to 7 days (T+168).

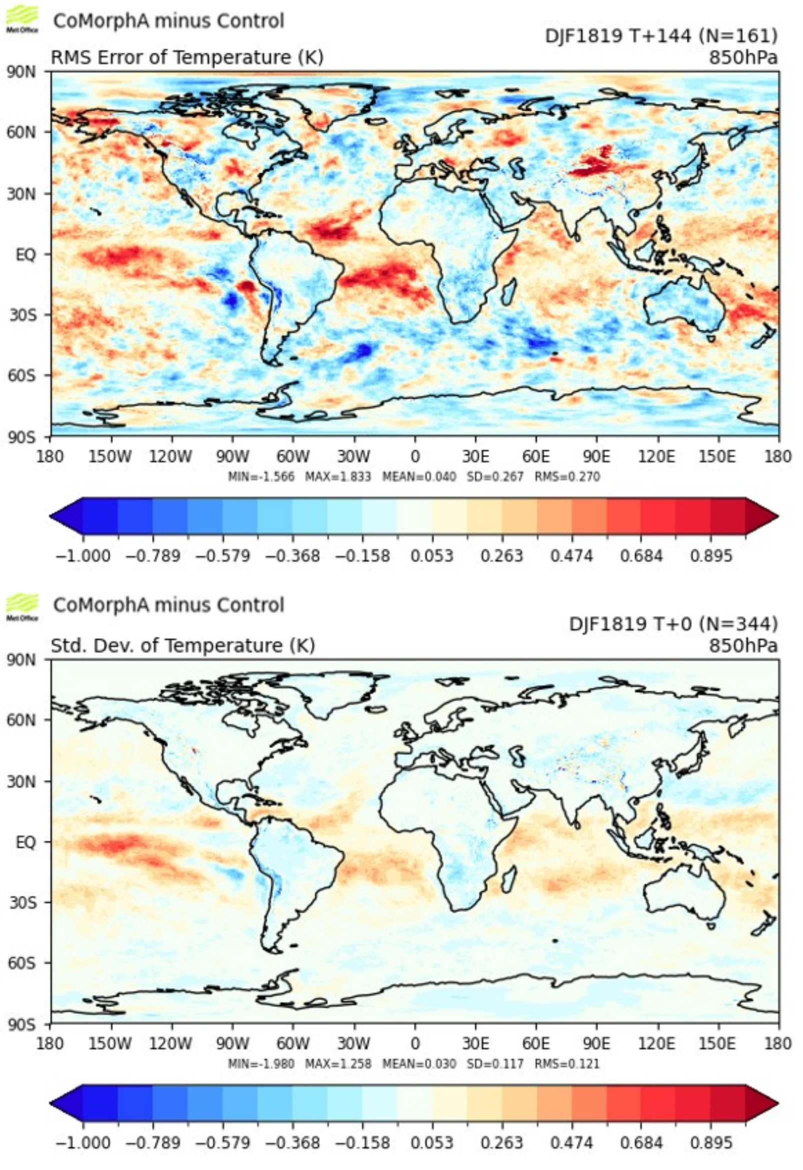

FIGURE 10 Change in root-mean-square error against own analysis of day 6 temperature at 850 hPa (top) and change in standard deviation of the analyses (bottom), from the winter NWP trials

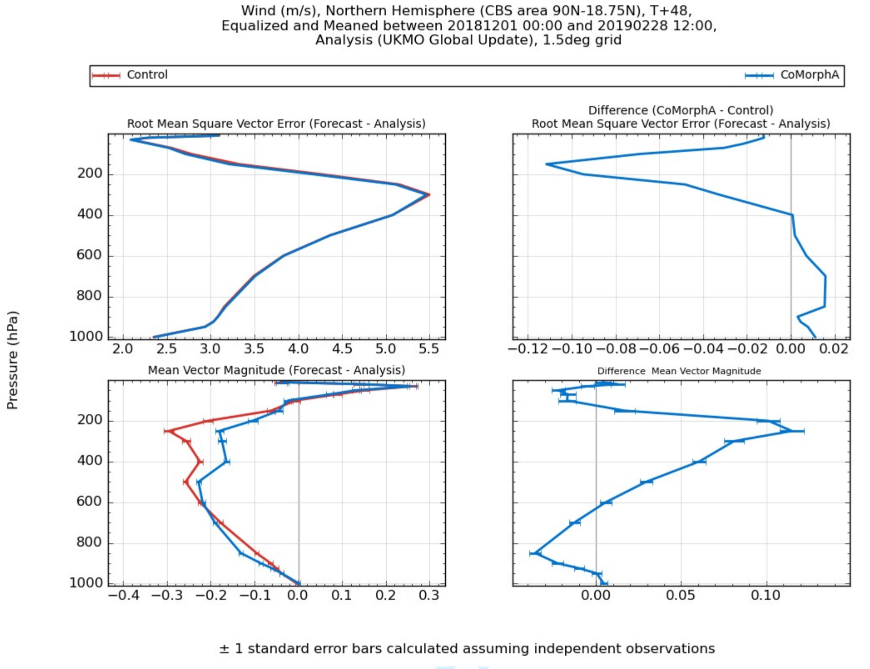

FIGURE 11 Profile of root mean square error (top left) and bias (bottom right) for northern hemisphere wind at T+48 of the DJF trial.

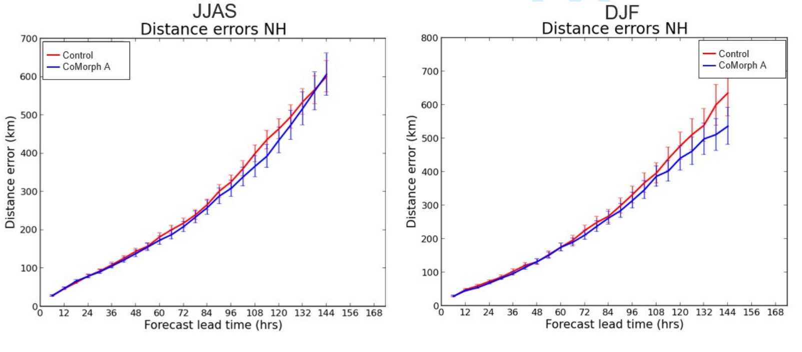

FIGURE 12 Extratropical cyclone track errors from the summer (left) and winter (right) NWP trials

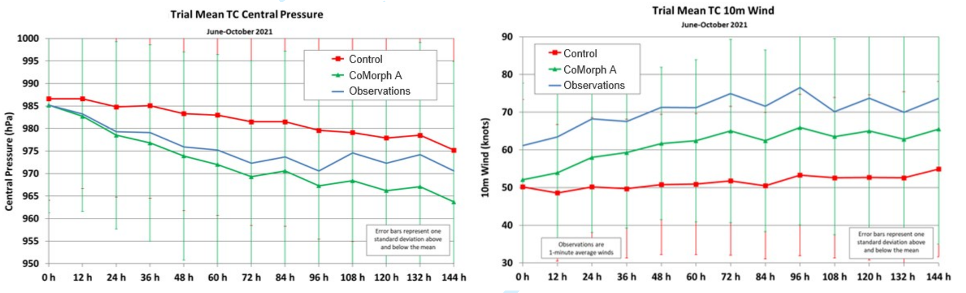

FIGURE 13 Tropical cyclone verification from the control and CoMorph-A forecasts at N1280 from June to October 2021

The performance of the CoMorph-A convection package in global simulations with the Met Office Unified Model

A. P. Lock, M.Whitall, A. J. Stirling, K. D.Williams, S. L. Lavender, C. Morcrette, K. Matsubayashi, P. R. Field, G. Martin, M.Willett, J. Heming

The new CoMorph-A package of physical parametrizations in the Met Office Unified Model is documented and shown to perform well in global configurations. The main component is an entirely new convection scheme, CoMorph, but it also includes significant changes to the cloud, microphysics and boundary layer parametrizations. Biases in radiative flux climatologies are significantly reduced (top panel for the control annual mean longwave cloud radiative forcing, bottom for CoMorph-A), tropical and extratropical cyclone statistics are improved, the MJO and other tropical waves are strengthened and it also improves overall scores in NWP trials.